Supercontinuum in ionization by relativistically intense and short laser pulses: Ionization without interference and its time analysis

K. Krajewska[1,2,*] and J. Z. Kamiński[1]

[1]*Institute of Theoretical Physics, Faculty of Physics, University of Warsaw, Pasteura 5, 02-093 Warsaw, Poland*

[2]*Department of Physics and Astronomy, University of Nebraska, Lincoln, Nebraska 68588-0299, USA*

(Received 3 August 2015; revised manuscript received 3 April 2016; published 5 July 2016)

Ionization by relativistically intense laser pulses of finite duration is considered in the framework of strong-field quantum electrodynamics. We show that the resulting ionization spectra change their behavior from the interference-dominated oscillatory pattern to the interference-free smooth supercontinuum, the latter being the main focus of this paper. More specifically, when studying the energy distributions of photoelectrons ionized by circularly polarized and short pulses, we observe the appearance of broad structures lacking the interference patterns. These supercontinua extend over hundreds of driving photon energies, thus corresponding to high-order nonlinear processes. Their positions on the electron energy scale can be controlled by changing the pulse duration. The corresponding polar-angle distributions show asymmetries which are attributed to the radiation pressure experienced by photoelectrons. Moreover, our time analysis shows that the electrons comprising the supercontinuum can form pulses of short duration. While we present the fully numerical results, their interpretation is based on the saddle-point approximation for the ionization probability amplitude.

DOI: 10.1103/PhysRevA.94.013402

I. INTRODUCTION

Interference of probability amplitudes is a fundamental quantum effect which, among others, manifests itself when a strong laser field interacts with matter. In his celebrated paper on strong-field ionization [1], Keldysh has shown how the probability amplitudes emerging from the complex-time saddle points lead to the interference pattern in the angular-energy distribution of photoelectrons. This idea, further developed for instance in [2,3] (for related recent investigations, see [4–6]), has initiated theoretical investigations of such quantum processes like the above-threshold ionization, the rescattering phenomenon, or the high-order harmonic generation. Along with important experimental achievements, it has led to a new branch of science called attosecond physics [7], which has already found a lot of applications in physics, chemistry, biology, and medicine. Some of these achievements are described in the review articles (see, e.g., [8–13]) or in the recent collection of articles [14] devoted to the Keldysh theory [15].

The Keldysh approach has been further generalized in order to account for the interaction of ionized electrons with their parent ions. This has led to the concept of complex-time trajectories (i.e., trajectories along complex time determined by the purely classical Newton equations) [16–18], or to the concept of quantum complex-time trajectories [19] which take into account the electron wave packet spreading or the quantum diffusion during the complex-time evolution, thus eliminating problems with the rescattering trajectories present in the former approach. Theoretical methods that have been developed from the ideas put forward by Keldysh are usually called the strong-field approximation (SFA) or the Keldysh-Faisal-Reiss (KFR) theory (see, also [20,21]). Recently, with the development of lasers generating relativistically intense and very short pulses, similar interference patterns have been investigated in the relativistic strong-field quantum electrodynamics [22–24]. In particular, such diverse phenomena have been studied as the vacuum polarization induced Young interference [25], the Kapitza-Dirac effect [26,27], interference effects in Compton and Thomson scattering (see, e.g., [28,29]), and in laser-modified Mott scattering [30,31], the coherent comb structures created by a finite train of short pulses in the Compton [32,33], Breit-Wheeler [34], and ionization [35] processes, which can be used for the diagnostics of relativistically intense laser pulses [36,37].

On the other hand, the lack of interference may result in an appearance of supercontinuum [38] which, since its demonstration in the early 1970s, has been the focus of significant research activities. The supercontinuum generation has attracted a lot of attention owing to its enormous spectral broadening. Thus, resulting in many useful applications, among others, in telecommunication and optical coherence tomography [39]. It has been shown in Ref. [40] that the supercontinuum in the radiation domain spreading over keV or MeV energy regions can be generated during the Thomson or Compton scattering. In light of this result, the following question arises: Is it possible to generate the supercontinuum in the ionization spectrum? In other words, is it possible to choose the parameters of a driving pulse such that the energy spectrum of photoelectrons does not change rapidly with energy, on the scale of tens or even hundreds of laser photon energies? In general, the answer to this question is negative as for even a few-cycle driving pulse the spectrum of photoelectrons consists of a sequence of peaks separated approximately by the laser carrier frequency (which, for monochromatic plane waves, are called the multiphoton peaks). The Keldysh theory shows that such a structure arises as the result of interference of at least two complex-time probability amplitudes. Thus, in order to create the supercontinuum, one should have a dominant complex-time saddle point with an imaginary part which, over a broad range of electron final energies, would be much smaller than imaginary parts of the remaining saddle

*katarzyna.krajewska@fuw.edu.pl

points. In other words, over a broad domain of electron final energies, interference of probability amplitudes should be suppressed. The aim of this paper is to show that, indeed, such a situation can happen in the relativistic ionization of atoms or positive ions by circularly polarized, short laser pulses.

We expect that the ionization supercontinuum can be used in various aspects of matter-wave optics. For instance, similar to the formation of attosecond pulses out of a broad energy spectrum of radiation, it may lead to the formation of very short electron bunches. Moreover, if the electron supercontinuum is produced by a train of pulses, it will result in the creation of coherent electron energy combs. In analogy to the radiation combs generated in Compton and Thomson scattering [28,29], this may lead to the synthesis of a sequence of very short "electron pulses." The latter could find applications in the "matter-wave" pump and probe electron scattering experiments, very similar to the ones already performed in optics. Finally, the formation of electron supercontinua and their angular distributions crucially depend on the parameters of the driving laser field (in particular, on its carrier envelope phase, the pulse shape, duration, and intensity). This opens a possibility of using the electron supercontinua in the diagnosis of extremely intense laser pulses, for which the conventional diagnostic methods (developed for moderately intense fields) fail. Note that the use of ionization spectra for diagnostic purposes was already proposed by Kalashnikov *et al.* in [41].

There is also a fundamental aspect related to the generation of electron supercontinua discussed in this paper. Namely, we show that for circularly polarized, short laser pulses of sufficiently large intensities, the spectrum of photoelectrons consists essentially of two, very distinctive structures. The first one occurs at low-electron energies and it is composed of peaks which, for long driving pulses, are interpreted as the multiphoton peaks. As it is already known, this low-energy structure results from interference of probability amplitudes emerging from different complex-time electron trajectories. A new aspect of our investigations is that, for intense and short driving pulses of a circular polarization, the second structure occurs. It is comparable in magnitude to the former one but it appears in the high-energy portion of the electron spectrum. Actually, its location on the electron energy scale can be controlled by changing the pulse duration. Moreover, it is smooth and broad as the interference effects are suppressed at these energies. Note that our predictions, which are based on the well-established Born approximation for the high-energy scattering state of electrons, could be studied experimentally in the future laser facilities (see, for instance, the European Light Inftrastructure (ELI) [42]).

In this paper, we use a very general definition of a laser pulse. Namely, we assume that the pulse lasts for a finite time T_p and has an arbitrary (but sufficiently smooth) time dependence. This is provided that the integral of the electric field component over time vanishes. The pulse duration allows us to introduce the so-called fundamental frequency $\omega = 2\pi/T_p$. Although it is not necessary, we also assume that the pulse consists of a well-defined number of electric field cycles, which we denote as $N_{\rm osc}$. This leads to the definition of the so-called laser carrier frequency $\omega_L = N_{\rm osc}\omega$. While this is an extra assumption used in our numerical illustrations, the theory presented here applies to arbitrary pulses for which the number of cycles $N_{\rm osc}$ as well as the laser carrier frequency ω_L cannot, in general, be defined. In particular, this method can be used in the analysis of ionization by arbitrary chirped pulses or by pulses with many laser carrier frequencies, not necessarily commensurate with respect to each other.

The organization of this paper is as follows. In Sec. II, we present the theoretical formulation of relativistic ionization based on the Dirac equation and with the full account for the spin degrees of freedom. Specifically, in Sec. II A we develop a general approach, which for the velocity gauge is elaborated in detail in Sec. II B. The supplementary Sec. II C is devoted to the analysis of saddle points arising from our formulation, which further is used *only* for the interpretation of numerical results. In Sec. III, we present numerical analysis of ionization of He^+ ions by short, circularly polarized, and relativistically intense pulses defined in Sec. III A. The energy and angular probability distributions are presented in Sec. III B, where also the generation of ionization supercontinua is discussed. Section III C is devoted to the further analysis of the supercontinuum with the result that it can be shifted towards high energies by changing the azimuthal angle of emission. In Sec. III D, we study the energy dependence of the phase of probability amplitudes and show in Sec. III E how the nearly linear dependence of the phase on the energy of emitted electrons leads to the time delay of the electron wave packets synthesized from a particular supercontinuum. In Sec. III F, we discuss properties of the probability distribution of ionization in a broader range of final electron energies. We demonstrate that the spectrum consists of the low-energy structure (which is dominated by the interference effects) and of the smooth and broad high-energy structure (i.e., the supercontinuum), being separated by the region of a very small ionization yield. As shown in Sec. III G, the supercontinuum can be controlled by changing the duration of a driving pulse. It results in its significant shift toward higher electron energies for shorter pulses. Such an unexpected behavior of the ionization distribution appears only for the circularly polarized, short laser pulses. For comparison, in Appendix A, ionization yield by a linearly polarized, short laser pulse is studied. In Sec. IV, we draw some concluding remarks. Appendixes B and C contain, respectively, supplementary materials concerning the physical units and the normalization of the laser pulse shape functions. Based on the Monte Carlo simulations, an estimation of the total ionization probability for circularly polarized pulses is presented in Appendix D.

Throughout the paper, we keep $\hbar = 1$. Hence, the fine-structure constant equals $\alpha = e^2/(4\pi\varepsilon_0 c)$. In numerical analysis we use relativistic units (rel. units) such that $\hbar = m_e = c = 1$ where m_e is the electron rest mass. We denote the product of any two four-vectors a^μ and b^μ as $a \cdot b = a^\mu b_\mu = a^0 b^0 - a^1 b^1 - a^2 b^2 - a^3 b^3$ $(\mu = 0,1,2,3)$, where the Einstein summation convention is used. For the four-vectors we use both the contravariant (a^0,a^1,a^2,a^3) and the standard $(a_0,a_x,a_y,a_z) = (a_0,\boldsymbol{a})$ notations. We employ the Feynman notation $\not{a} = \gamma \cdot a = \gamma^\mu a_\mu$ for the contraction with the Dirac matrices γ^μ and use a customary notation $\bar{u} = u^\dagger \gamma^0$, where $u^\dagger$ is the Hermitian conjugate of a bispinor u. Finally, we use the so-called light-cone variables. Namely, for a given space direction determined by a unit vector $\boldsymbol{n}$ (which in our paper is the direction of the laser pulse propagation) and for an arbitrary

four-vector a, we keep the following notations: $a^{\parallel} = \boldsymbol{n}\cdot\boldsymbol{a}$, $a^{-} = a^{0} - a^{\parallel}$, $a^{+} = (a^{0} + a^{\parallel})/2$, and $\boldsymbol{a}^{\perp} = \boldsymbol{a} - a^{\parallel}\boldsymbol{n}$. Thus, $a\cdot b = a^{+}b^{-} + a^{-}b^{+} - \boldsymbol{a}^{\perp}\cdot\boldsymbol{b}^{\perp}$ and $d^{4}x = dx^{+}dx^{-}d^{2}x^{\perp}$.

II. THEORY AND APPROXIMATIONS

A. General theory

The relativistic ionization of one-electron atoms or ions is described by the Dirac equation ($e = -|e|$)

$$[i\gamma^{\nu}\partial_{\nu} - e\gamma^{\nu}\mathcal{A}_{\nu}(x) - m_{e}c]\Psi(x) = 0. \tag{1}$$

The electromagnetic potential $\mathcal{A}(x)$ is assumed to be of the form

$$\mathcal{A}^{\nu}(x) = \frac{1}{ec}V(\boldsymbol{x})\delta^{\nu}{}_{0} + A^{\nu}_{R}(x), \tag{2}$$

where $V(\boldsymbol{x})$ is the binding potential and $A^{\nu}_{R}(x)$ describes the laser pulse. The analysis of the time evolution of the system leads to the exact expression for the probability amplitude

$$\mathcal{A}_{\mathrm{fi}} = -i\int d^{4}x\, e^{-i(E_{0}/c)x^{0}}\bar{\Psi}_{\mathrm{f}}(x)e\not{A}_{R}(x)\Psi_{\mathrm{i}}(\boldsymbol{x}). \tag{3}$$

Here, the bispinor $\Psi_{\mathrm{i}}(\boldsymbol{x})$ describes the electron bound state of energy E_{0} and $\Psi_{\mathrm{f}}(x)$ is the exact solution of Eq. (1) corresponding to the scattering state with the incoming spherical waves.

Although the analytic form of $\Psi_{\mathrm{i}}(\boldsymbol{x})$ is known for the Coulomb potential, the exact solution $\Psi_{\mathrm{f}}(x)$ can be determined only numerically. Recently, we observe a significant progress in solving numerically the relativistic Dirac equation (see, e.g., Refs. [43–47]). Even so, for very large intensities of laser pulses available today (of the order of 10^{20} W/cm^{2} and larger) and for high energies of photoelectrons (i.e., a few keV and higher) such solutions are not achievable. If, however, the exact scattering state is labeled by the asymptotic momentum $\boldsymbol{p}$ for which the kinetic energy $\sqrt{(m_{e}c^{2})^{2} + (c\boldsymbol{p})^{2}} - m_{e}c^{2}$ is much larger than the ionization potential of the initial bound state $m_{e}c^{2} - E_{0}$, then for the final scattering state the Born expansion with respect to the static potential $V(\boldsymbol{x})$ can be applied. This is the essence of the relativistic SFA which, in the lowest order, consists in replacing in Eq. (3) the exact solution $\Psi_{\mathrm{f}}(x)$ of Eq. (1) by the corresponding exact solution of the simplified Dirac equation

$$[i\not{\partial} - e\not{A}_{R}(x) - m_{e}c]\Psi^{(0)}_{\mathrm{f}}(x) = 0. \tag{4}$$

For the relativistic SFA approach to ionization by plane-wave fields, we refer the reader to [48–53]. In this paper, however, we focus on relativistic ionization by finite laser pulses.

Let us choose as the solution of (4), denoted since now on by $\Psi^{(0)}_{\boldsymbol{p}\lambda}(x)$, the one with the well-defined electron momentum $\boldsymbol{p}$ and spin polarization $\lambda = \pm$. The probability amplitude $\mathcal{A}_{\mathrm{fi}}$ (3), which in this case we denote as $\mathcal{A}(\boldsymbol{p},\lambda;\lambda_{\mathrm{i}})$, becomes

$$\mathcal{A}(\boldsymbol{p},\lambda;\lambda_{\mathrm{i}}) = -i\int\frac{d^{3}q}{(2\pi)^{3}}\int d^{4}x\, e^{-iq\cdot x}\bar{\Psi}^{(0)}_{\boldsymbol{p}\lambda}(x)e\not{A}_{R}(x)\tilde{\Psi}_{\mathrm{i}}(\boldsymbol{q}), \tag{5}$$

where

$$\Psi_{\mathrm{i}}(\boldsymbol{x}) = \int\frac{d^{3}q}{(2\pi)^{3}}e^{i\boldsymbol{q}\cdot\boldsymbol{x}}\tilde{\Psi}_{\mathrm{i}}(\boldsymbol{q}). \tag{6}$$

To shorten the notation, we have introduced $q = (q^{0},\boldsymbol{q}) = (E_{0}/c,\boldsymbol{q})$. Note that it is not the four-vector as it does not transform properly under the relativistic Lorentz transformations. Nevertheless, for the sake of space, we shall call it the four-momentum as it is usually done for the electromagnetic potential $A^{\nu}_{R}(x)$ in the Dirac equation (1), which is the four-vector only for particular gauges. In addition, λ_{i} labels the spin degrees of freedom for the initial state.

Even after this approximation, the direct numerical analysis of Eq. (5) is not possible as, for the laser pulses concentrated in a finite focus region, the numerical solution of Eq. (4) is not available for laser pulse and electron parameters mentioned above. For this reason, the so-called plane-wave front approximation for the laser beam is applied. It accounts for the finite time and space dependence of the laser pulse in the direction of its propagation, however, in the space directions perpendicular to the propagation direction it is assumed that the laser field extends to infinities. Such an approximation is justified if either the laser pulse is not tightly focused or interaction takes place with the highly energetic beams of particles, atoms, or ions in the head-on kinematics (see, e.g., Ref. [54]). Note that this approximation is commonly used in majority of investigations of quantum processes in strong laser fields, as only in this case it is possible to obtain the exact analytical solution of the Dirac equation, called the Volkov solution [55].

B. Velocity gauge

In nonrelativistic SFA one usually considers probability amplitudes in two gauges: the velocity and length gauges. The same is possible in the relativistic case. In this paper, we consider the velocity gauge, postponing the consideration of the length gauge to the near future.

In order to derive the corresponding formulas, let us consider the most general form (up to the gauge transformation) of the electromagnetic potential in the plane-wave front approximation

$$A_{R}(x) \equiv A(\phi) = A_{0}[\varepsilon_{1}f_{1}(\phi) + \varepsilon_{2}f_{2}(\phi)], \tag{7}$$

where $\phi = k\cdot x = k^{0}x^{-}$, $k = k^{0}n = k^{0}(1,\boldsymbol{n})$, $k^{0} = \omega/c$, $\omega = 2\pi/T_{p}$, ε_{j} are two real polarization four-vectors normalized such that $\varepsilon_{j}\cdot\varepsilon_{j'} = -\delta_{jj'}$ and perpendicular to the propagation direction of the laser pulse, $k\cdot\varepsilon_{j} = 0$. Here, we have also introduced T_{p} for the pulse duration. The two real functions $f_{j}(\phi)$, called the shape functions, are arbitrary functions with the continuous second derivatives that vanish for $\phi < 0$ and $\phi > 2\pi$. Introducing the relativistically invariant parameter

$$\mu = \frac{|eA_{0}|}{m_{e}c}, \tag{8}$$

that defines the intensity of the laser field (the relation between this parameter and the time-averaged intensity of the laser pulse is presented in the Appendix B), we rewrite (7) as

$$eA(\phi) = -m_{e}c\mu[\varepsilon_{1}f_{1}(\phi) + \varepsilon_{2}f_{2}(\phi)]. \tag{9}$$

Hence, the Dirac equation (4) becomes

$$\{i\not{\partial} + m_{e}c\mu[\not{\varepsilon}_{1}f_{1}(\phi) + \not{\varepsilon}_{2}f_{2}(\phi)] - m_{e}c\}\Psi(x) = 0. \tag{10}$$

We denote as $\psi^{(+)}_{\boldsymbol{p}\lambda}(x)$ the Volkov solution of this equation for electrons [the superscript (+) means that it is a positive-energy solution], where $\boldsymbol{p}$ is the electron asymptotic momentum and $\lambda = \pm$ labels the spin degrees of freedom. Its explicit form can be written as [56]

$$\psi^{(+)}_{\boldsymbol{p}\lambda}(x) = \sqrt{\frac{m_e c^2}{V E_{\boldsymbol{p}}}}\Big\{1 + \frac{m_e c\mu}{2p\cdot k}[f_1(k\cdot x)\not{\varepsilon}_1\not{k} + f_2(k\cdot x)\not{\varepsilon}_2\not{k}]\Big\} e^{-iS^{(+)}_p(x)} u^{(+)}_{\boldsymbol{p}\lambda}, \tag{11}$$

where

$$S^{(+)}_p(x) = p\cdot x + \int_0^{k\cdot x} d\phi\left\{-\frac{m_e c\mu}{p\cdot k}[\varepsilon_1\cdot p f_1(\phi) + \varepsilon_2\cdot p f_2(\phi)] + \frac{(m_e c\mu)^2}{2p\cdot k}\left[f_1^2(\phi) + f_2^2(\phi)\right]\right\}. \tag{12}$$

Here, the photoelectron asymptotic energy equals $E_{\boldsymbol{p}} = \sqrt{(c\boldsymbol{p})^2 + (m_e c^2)^2}$ whereas the on-mass-shell four-vector is $p = (p^0, \boldsymbol{p}) = (E_{\boldsymbol{p}}/c, \boldsymbol{p})$. The Dirac free-particle bispinors $u^{(+)}_{\boldsymbol{p}\lambda}$ are normalized such that $\bar{u}^{(+)}_{\boldsymbol{p}\lambda} u^{(+)}_{\boldsymbol{p}\lambda'} = \delta_{\lambda\lambda'}$, and V is the quantization volume. With this normalization the final density of electron states, for a given spin degree of freedom, is equal to $V d^3p/(2\pi)^3$.

For our further purposes, we introduced the following functions [the explicit form of the ground-state wave functions $\Psi_{\mathrm{i}}(\boldsymbol{x})$ for the hydrogenlike ions and for two spin polarizations can be found in the textbook [57]]:

$$\begin{aligned} B^{(0,0)}_{\boldsymbol{p}\lambda;\lambda_{\mathrm{i}}}(\boldsymbol{q}) &= \bar{u}^{(+)}_{\boldsymbol{p}\lambda}\not{n}\tilde{\Psi}_{\mathrm{i}}(\boldsymbol{q}),\\ B^{(1,0)}_{\boldsymbol{p}\lambda;\lambda_{\mathrm{i}}}(\boldsymbol{q}) &= \bar{u}^{(+)}_{\boldsymbol{p}\lambda}\not{\varepsilon}_1\tilde{\Psi}_{\mathrm{i}}(\boldsymbol{q}),\\ B^{(0,1)}_{\boldsymbol{p}\lambda;\lambda_{\mathrm{i}}}(\boldsymbol{q}) &= \bar{u}^{(+)}_{\boldsymbol{p}\lambda}\not{\varepsilon}_2\tilde{\Psi}_{\mathrm{i}}(\boldsymbol{q}). \end{aligned} \tag{13}$$

This allows us to represent the probability amplitude (5) in the form (note that $\not{\varepsilon}_j\not{k}\not{\varepsilon}_j = \not{k}$, for $j = 1,2$, and $\not{\varepsilon}_1\not{k}\not{\varepsilon}_2 + \not{\varepsilon}_2\not{k}\not{\varepsilon}_1 = 0$)

$$\mathcal{A}(\boldsymbol{p},\lambda;\lambda_{\mathrm{i}}) = \int \frac{d^3q}{(2\pi)^3}\int d^4x\, e^{iS^{(+)}_p(x) - iq\cdot x} M(k\cdot x), \tag{14}$$

with

$$M(k\cdot x) = im_e c\mu\sqrt{\frac{m_e c^2}{V E_{\boldsymbol{p}}}}\Big(f_1(k\cdot x)B^{(1,0)}_{\boldsymbol{p}\lambda;\lambda_{\mathrm{i}}}(\boldsymbol{q}) + f_2(k\cdot x)B^{(0,1)}_{\boldsymbol{p}\lambda;\lambda_{\mathrm{i}}}(\boldsymbol{q}) - \frac{m_e c\mu}{2p\cdot n}\{[f_1(k\cdot x)]^2 + [f_2(k\cdot x)]^2\}B^{(0,0)}_{\boldsymbol{p}\lambda;\lambda_{\mathrm{i}}}(\boldsymbol{q})\Big). \tag{15}$$

Next, we introduce the so-called laser-dressed momentum [58–60]

$$\bar{p} = p - \frac{m_e c\mu}{p\cdot k}(\varepsilon_1\cdot p\langle f_1\rangle + \varepsilon_2\cdot p\langle f_2\rangle)k + \frac{(m_e c\mu)^2}{2p\cdot k}\left(\left\langle f_1^2\right\rangle + \left\langle f_2^2\right\rangle\right)k, \tag{16}$$

where, for any continuous function $F(\phi)$, that vanishes outside the interval $0 \leqslant \phi \leqslant 2\pi$, we define

$$\langle F\rangle = \frac{1}{2\pi}\int_0^{2\pi} d\phi\, F(\phi). \tag{17}$$

The dressed momentum fulfills the equations

$$\bar{p}^- = p^- \quad \text{and} \quad \bar{\boldsymbol{p}}^\perp = \boldsymbol{p}^\perp, \tag{18}$$

that allow us to write

$$S^{(+)}_p(x) = \bar{p}^+ x^- + p^- x^+ - \boldsymbol{p}^\perp\cdot\boldsymbol{x}^\perp + G_p(k^0 x^-), \tag{19}$$

where

$$G_p(\phi) = \int_0^\phi d\phi'\Big(-\frac{m_e c\mu}{p\cdot k}\{\varepsilon_1\cdot p[f_1(\phi') - \langle f_1\rangle] + \varepsilon_2\cdot p[f_2(\phi') - \langle f_2\rangle]\} + \frac{(m_e c\mu)^2}{2p\cdot k}\left[f_1^2(\phi') - \left\langle f_1^2\right\rangle + f_2^2(\phi') - \left\langle f_2^2\right\rangle\right]\Big). \tag{20}$$

Inserting (19) into (14) we see that the integrations over dx^+ and $d^2x^\perp$ lead to the conservation conditions

$$p^- = q^- \quad \text{and} \quad \boldsymbol{p}^\perp = \boldsymbol{q}^\perp, \tag{21}$$

that permit us to carry out the integration over d^3q. The remaining integration over dx^- is performed by applying the following Fourier decompositions for $j = 1,2$ and $0 \leqslant \phi = k^0 x^- \leqslant 2\pi$:

$$[f_1(\phi)]^j \exp[iG_p(\phi)] = \sum_{N=-\infty}^{\infty} G_N^{(j,0)} e^{-iN\phi}, \tag{22}$$

$$[f_2(\phi)]^j \exp[iG_p(\phi)] = \sum_{N=-\infty}^{\infty} G_N^{(0,j)} e^{-iN\phi}. \tag{23}$$

This allows us to write the probability amplitude in the form

$$\mathcal{A}(\boldsymbol{p},\lambda;\lambda_i) = im_e c\mu\sqrt{\frac{m_e c^2}{V E_{\boldsymbol{p}}}}\mathcal{D}(\boldsymbol{p},\lambda;\lambda_{\mathrm{i}}), \tag{24}$$

with

$$\mathcal{D}(\boldsymbol{p},\lambda;\lambda_{\mathrm{i}}) = \sum_{N=-\infty}^{\infty}\frac{e^{2\pi i(\bar{p}^+ - q^+ - Nk^0)/k^0} - 1}{i(\bar{p}^+ - q^+ - Nk^0)} \times\Big\{G_N^{(1,0)}B^{(1,0)}_{\boldsymbol{p}\lambda;\lambda_{\mathrm{i}}}(\boldsymbol{Q}) + G_N^{(0,1)}B^{(0,1)}_{\boldsymbol{p}\lambda;\lambda_{\mathrm{i}}}(\boldsymbol{Q}) - \frac{m_e c\mu}{2p\cdot n}\left[G_N^{(2,0)} + G_N^{(0,2)}\right]B^{(0,0)}_{\boldsymbol{p}\lambda;\lambda_{\mathrm{i}}}(\boldsymbol{Q})\Big\} \tag{25}$$

and

$$\boldsymbol{Q} = \boldsymbol{p} + (q^0 - p^0)\boldsymbol{n}. \tag{26}$$

Note that in the corresponding nonrelativistic SFA and with the dipole approximation applied to the laser field, the momentum $\boldsymbol{Q}$ in Eq. (26) is not shifted by the vector $(q^0 - p^0)\boldsymbol{n}$, independently of the gauge choice. This term, among others, is responsible for the so-called radiation pressure [61] which has recently been discussed in the literature (see, e.g., [47,62–67]).

Such a momentum shift appears also in the so-called Coulomb-corrected relativistic SFA [see, e.g., Eq. (24) in Ref. [53]].

Equation (25) allows us to define the most probable energy absorbed by photoelectrons during the ionization. Namely, the ionization probability distribution is maximum for such N for which the denominator $\bar{p}^+ - q^+ - Nk^0$ takes the smallest values. This happens for those N which are as close as possible to the number

$$N_{\rm eff} = \frac{c\bar{p}^+ - cq^+}{\omega}. \tag{27}$$

Hence, the energy which is most probably transferred from the pulse to the atomic or ionic system during the ionization equals

$$E_{\rm tr} = N_{\rm eff}\omega. \tag{28}$$

Note that both quantities $N_{\rm eff}$ and $E_{\rm tr}$ are gauge invariant [59]. Moreover, $N_{\rm eff}$ is Lorentz invariant for relativistically covariant processes.

Finally, the total spin-fixed probability of ionization equals

$$P(\lambda;\lambda_{\rm i}) = \mu^2\frac{(m_e c)^3}{(2\pi)^3}\int\frac{d^3p}{p^0}|\mathcal{D}(\boldsymbol{p},\lambda;\lambda_{\rm i})|^2, \tag{29}$$

whereas its triply differential distribution takes the form

$$\frac{d^3P(\boldsymbol{p},\lambda;\lambda_{\rm i})}{dE_{\boldsymbol{p}}d^2\Omega_{\boldsymbol{p}}} = \mu^2\frac{(m_e c)^3}{(2\pi)^3 c}|\boldsymbol{p}|\cdot|\mathcal{D}(\boldsymbol{p},\lambda;\lambda_{\rm i})|^2. \tag{30}$$

We see that in the last two formulas the quantization volume V cancels. For the purpose of numerical illustrations let us introduce the dimensionless distribution

$$\mathcal{P}_{\lambda_{\rm i}\lambda}(\boldsymbol{p}) = \alpha^2 m_e c^2\frac{d^3P(\boldsymbol{p},\lambda;\lambda_{\rm i})}{dE_{\boldsymbol{p}}d^2\Omega_{\boldsymbol{p}}}, \tag{31}$$

which is the probability distribution in the atomic units. Later on, we shall label the spin degrees of freedom as $\downarrow$ and $\uparrow$ for λ or $\lambda_{\rm i}$ equal to $-$ and $+$, respectively.

In this section, we have derived formulas for the energy-angular probability distributions that are valid *only* for sufficiently large electron kinetic energies $E_{\rm kin}$, for which the condition

$$E_{\rm kin} = \sqrt{(m_e c^2)^2 + (c\boldsymbol{p})^2} - m_e c^2 \gg m_e c^2 - E_0 \tag{32}$$

is satisfied. Thus, we shall apply current theory to ionization of He^+ ions, with the ionization potential of roughly 54 eV, and we will analyze the energy-angular probability distributions for final electron kinetic energies larger than 1 keV. It is also commonly assumed that the SFA is applicable for sufficiently intense laser fields, specifically, when the ponderomotive energy is larger or comparable to the ionization potential. This condition is also very well fulfilled in our numerical analysis.

C. Saddle-point analysis

Expressions for the energy-angular probability distribution of photoelectrons, which have been derived in the previous section, are not convenient for the interpretation of calculated results. On the other hand, a very appealing interpretation can be provided by analyzing the saddle points of the corresponding integrands, as it has been suggested by Keldysh. The latter has been applied, for instance, in Refs. [4,19] in investigations of the diffraction and interference structures in the probability distributions. As the formulas presented above do not suit for such an analysis, therefore, we have to rewrite the expression for the probability amplitude $\mathcal{A}(\boldsymbol{p},\lambda;\lambda_{\rm i})$ in a different form. For this purpose, we present (14) in the light-cone variables as

$$\begin{aligned}\mathcal{A}(\boldsymbol{p},\lambda;\lambda_{\rm i}) = \frac{1}{k^0}\int_0^{2\pi}d\phi\int\frac{d^3q}{(2\pi)^3}\int dx^+d^2x^\perp \\ \times e^{i(p^- - q^-)x^+ - i(\boldsymbol{p}^\perp - \boldsymbol{q}^\perp)\cdot\boldsymbol{x}^\perp} \\ \times e^{iG(g_0,g_1,g_2,h;\phi)}M(\phi),\end{aligned} \tag{33}$$

where $M(\phi)$ is defined by (15) and

$$\begin{aligned}G(g_0,g_1,g_2,h;\phi) = \int_0^\phi d\phi'\big\{g_0 + g_1 f_1(\phi') + g_2 f_2(\phi') \\ + h\big[f_1^2(\phi') + f_2^2(\phi')\big]\big\},\end{aligned} \tag{34}$$

with

$$\begin{aligned}g_0 = \frac{p^+ - q^+}{k^0},\quad g_j = -m_{\rm e}c\mu\frac{\varepsilon_j\cdot p}{k\cdot p},\quad j = 1,2, \\ h = \frac{(m_{\rm e}c\mu)^2}{2k\cdot p}.\end{aligned} \tag{35}$$

Since the integrations over $dx^+d^2x^\perp$ lead to the conservation conditions (21), we end up with the following expression for the probability amplitude:

$$\mathcal{A}(\boldsymbol{p},\lambda;\lambda_{\rm i}) = \frac{1}{k^0}\int_0^{2\pi}d\phi\, e^{iG(g_0,g_1,g_2,h;\phi)}[M(\phi)]_{\boldsymbol{q}=\boldsymbol{Q}}, \tag{36}$$

where $\boldsymbol{Q}$ is defined in Eq. (26). This is the formula which suits for the saddle-point analysis. In the following, if it does not lead to misunderstandings, we abbreviate the function $G(g_0,g_1,g_2,h;\phi)$ by $G(\phi)$. Let us also note that, due to the conservation conditions (21), g_0 in (35) equals

$$g_0 = \frac{p^0 - q^0}{k^0}, \tag{37}$$

and it depends only on energies of the initial and final states.

Applying now the standard asymptotic procedure for the approximate evaluation of integrals, we determine the saddle points by solving the equation

$$G'(\phi) = 0, \tag{38}$$

where *prime* means the derivative over ϕ. This equation has in general complex solutions. Among them we select only those saddle points, denoted by ϕ_s, for which $\mathrm{Im}\,G(\phi_s) > 0$. Hence, we arrive at the approximate expression for the probability amplitude

$$\mathcal{A}(\boldsymbol{p},\lambda;\lambda_{\rm i}) = \frac{1}{k^0}\sum_s e^{iG(\phi_s)}\sqrt{\frac{2\pi i}{G''(\phi_s)}}[M(\phi_s)]_{\boldsymbol{q}=\boldsymbol{Q}}. \tag{39}$$

If $[M(\phi)]_{\boldsymbol{q}=\boldsymbol{Q}}$ is singular at the saddle point, we have to apply the so-called singular saddle-point approximation described, for instance, in Refs. [3,18,19]. However, independently of the method applied, the dominant behavior of the integral (36) is determined by the exponent $e^{iG(\phi_s)}$ which usually, for high-energy electrons, decays very fast to 0. Moreover,

the analysis of such integrals shows that in most cases at least two saddle points contribute significantly to the above sum, which results in the interference pattern observed in the probability distributions. At this point, let us emphasize that it is not our aim to compare the results predicted by the exact formula (30) with the ones that follow from the saddle-point approximation (39). We treat the expression (39) only as the appealing interpretative tool for our numerical analysis.

Equation (39) suggests that the interference pattern in ionization is suppressed (i.e., the ionization supercontinuum may appear) if there is only one saddle point for which, over a broad range of electron energies, Im $G(\phi_s)$ is much smaller than the corresponding values for the remaining saddle points. We shall see below that such a situation can indeed take place. Note that conclusions which follow from this interpretation are gauge independent, as only the function $M(\phi)$ depends on the chosen gauge.

III. NUMERICAL ANALYSIS

A. Pulse shape

The laser pulse with the $\sin^2$ envelope considered in this paper is defined as follows. First, we introduce two angles

$$\delta_j = (j-1)\frac{\pi}{2}, \quad j = 1,2 \tag{40}$$

and two functions

$$F_j(\phi) = F_0(\phi,\delta_j,\chi)\cos(\delta+\delta_j), \tag{41}$$

with

$$F_0(\phi,\delta_j,\chi) = N_0 \sin^2\left(\frac{\phi}{2}\right)\sin(N_{\rm osc}\phi+\delta_j+\chi) \tag{42}$$

for $0<\phi<2\pi$ and 0 otherwise. Next, we define the shape functions $f_j(\phi)$ of the electromagnetic vector potential (9) as

$$f_j(\phi) = -\int_0^\phi d\phi' F_j(\phi'). \tag{43}$$

This means that Eq. (42) defines the space and time dependence of the pulse. To be more specific, we have that for $0 < t - \boldsymbol{n}\cdot\boldsymbol{r}/c < T_p$,

$$\begin{aligned} F_0(\boldsymbol{r},t,\delta_j,\chi) &= N_0 \sin^2\left[\frac{1}{2}\omega(t-\boldsymbol{n}\cdot\boldsymbol{r}/c)\right] \\ &\quad\times \sin[N_{\rm osc}\omega(t-\boldsymbol{n}\cdot\boldsymbol{r}/c)+\delta_j+\chi] \\ &= N_0 \sin^2\left[\frac{1}{2N_{\rm osc}}\omega_L(t-\boldsymbol{n}\cdot\boldsymbol{r}/c)\right] \\ &\quad\times \sin[\omega_L(t-\boldsymbol{n}\cdot\boldsymbol{r}/c)+\delta_j+\chi], \end{aligned} \tag{44}$$

and it is 0 otherwise.

Since for $N_{\rm osc} > 1$ the Fourier decompositions of $F_j(\phi)$ do not contain constant terms, the above definitions of $f_j(\phi)$ guarantee that also for $\phi > 2\pi$ the vector potential vanishes. The physical interpretation of the remaining parameters is as follows. The angle δ determines the polarization properties of the laser pulse and, for the circularly polarized field, we choose $\delta = \pi/4$. The carrier envelope phase χ is assumed to be $\pi/2$. Finally, N_0 is the normalization-dependent real and positive factor which is chosen such that the normalization condition (B2) is fulfilled (for details, see Appendix C). The integer $N_{\rm osc}$ defines the number of cycles in the pulse and it is assumed to be equal to 4. The laser pulse propagates in the z direction [$\boldsymbol{k} = (\omega/c)\boldsymbol{n}$, $\boldsymbol{n} = \boldsymbol{e}_z$] and the real polarization vectors are equal to $\boldsymbol{\varepsilon}_1 = \boldsymbol{e}_x$ and $\boldsymbol{\varepsilon}_2 = \boldsymbol{e}_y$.

We consider here the interaction of a laser pulse with a positively charged He^+ ion, which is a one-electron ion with $Z = 2$. Since in our case the pulse is finite, therefore, the initial bound state is well defined. For this reason, we do not have to restrict our analysis to one-electron ions of very large Z, as it has been done in Refs. [51–53] where the infinite plane-wave field has been considered. Moreover, as the ion can have relativistic energy, we can choose the carrier frequency of the laser pulse ω_L freely. This is due to the fact that the calculations are carried out in the ion reference frame in which, for the head-on geometry of the ion and the laser beam, both the frequency and the electric-field strength are Doppler upshifted. This aspect has been originally discussed for the laser-induced Bethe-Heitler process in Ref. [68] (see, also the review articles [22,23]). For this reason, we assume that $\omega_L = N_{\rm osc}\omega = 20$ eV and the time-averaged intensity is $I = 10^{20}$ W/cm^2 (as it has been chosen for instance in Ref. [49]); in other words, we consider parameters which are experimentally available [69–71].

In Fig. 1, we present trajectories of the tips of vectors $\boldsymbol{A}(\phi)$ (upper panel) and $\boldsymbol{\mathcal{E}}(\phi) = -\partial_t \boldsymbol{A}(\phi)$ (lower panel) in the polarization plane xy, which is perpendicular to the direction of propagation of the laser pulse $\boldsymbol{n}$. The plots are in the relativistic units, with the units for the electromagnetic potential $A_S = m_e c/|e|$ and the electric field strength $\mathcal{E}_S = m_e c^2/(|e|\lambda\!\!\!^{-}_C) = m_e^2 c^3/|e|$; the latter is known as the Sauter-Schwinger critical field [72,73]. Hence, in Fig. 1, we present x and y components of the vectors $-\boldsymbol{A}(\phi)/A_S = e\boldsymbol{A}(\phi)/(m_e c)$ and $-\boldsymbol{\mathcal{E}}(\phi)/\mathcal{E}_S = e\boldsymbol{\mathcal{E}}(\phi)/(|e|\mathcal{E}_S)$.

The intensity of the laser pulse is considered to be relativistic if the time-averaged ponderomotive energy (see, e.g., [36])

$$U = -e^2\frac{\langle A\cdot A\rangle - \langle A\rangle\cdot\langle A\rangle}{2m_e} \tag{45}$$

is comparable to or larger than $m_e c^2$, or the amplitude of the electromagnetic potential is comparable to or larger than A_S. As follows from the upper panel of Fig. 1, for the chosen laser pulse parameters the laser pulse intensity can be considered as nearly relativistic.

B. Supercontinuum

Previously, the main reason to investigate ionization of atoms or ions within the relativistic quantum mechanics was to analyze the electron spin effects, not present in its nonrelativistic counterpart. It has been shown in Ref. [49] that the spin-flipping processes, in which the electron initial and final spins both projected on the same direction in space (usually chosen as the direction of propagation of the laser pulse) are opposite to each other, are less probable by roughly two orders of magnitude (i.e., of the order of the fine-structure constant α) as compared to the ionization processes in which the projections of the initial and final electron spins are conserved. Our numerical analysis confirms these findings

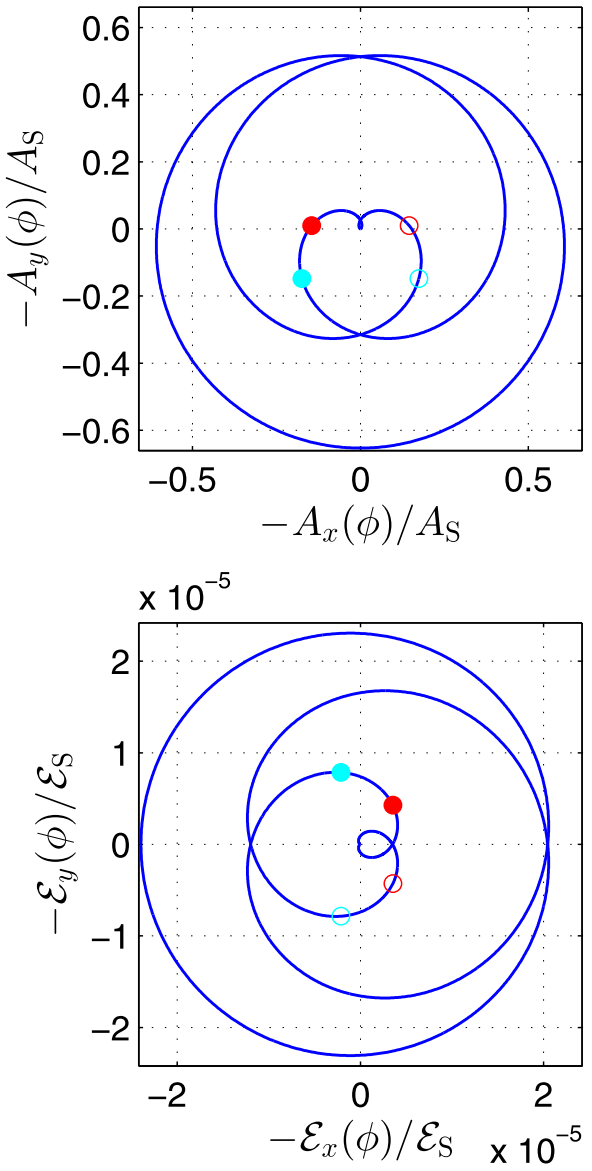

FIG. 1. Trajectories of the tips of the electromagnetic vector potential $\boldsymbol{A}(\phi)$ (upper panel) and the electric field vector $\boldsymbol{\mathcal{E}}(\phi)$ (lower panel) in the relativistic units for the laser pulse parameters discussed in detail in Sec. III A. All trajectories start from and end up at the origin (0,0). In order to show the direction of the time evolution, we mark with the filled and open circles the points on these trajectories corresponding to some particular values of ϕ: red (dark) filled circle for $\phi = 0.32\pi$, cyan (gray) filled circle for $\phi = 0.396\pi$, cyan (gray) open circle for $\phi = 2\pi - 0.396\pi$, and red (dark) open circle for $\phi = 2\pi - 0.32\pi$. The meaning of these particular points is discussed in the text. We observe the azimuthal symmetry of the electromagnetic potential $\varphi \to \pi - \varphi \bmod 2\pi$ or $(x,y) \to (-x,y)$, and of the electric field $\varphi \to -\varphi \bmod 2\pi$ or $(x,y) \to (x,-y)$.

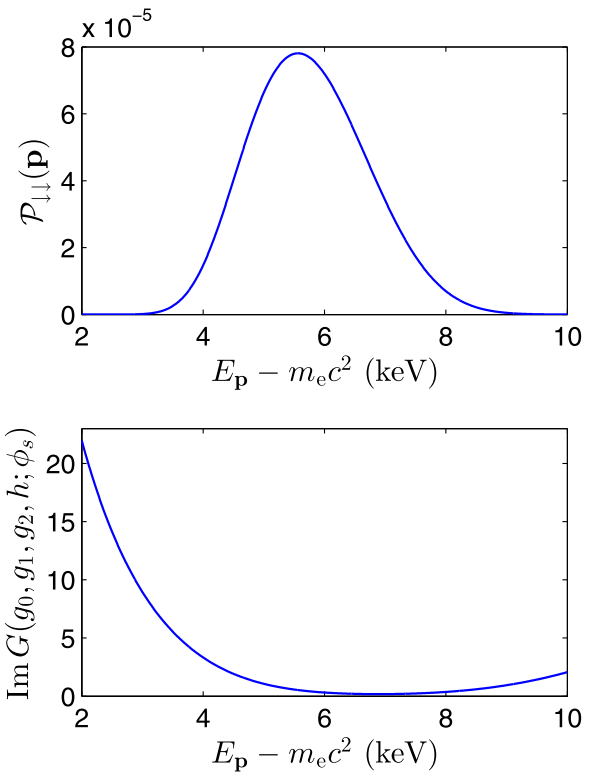

FIG. 2. The ionization probability $\mathcal{P}_{\downarrow\downarrow}(\boldsymbol{p})$ (upper panel) of He^+ ions for $\theta_p = 0.48\pi$ and $\varphi_p = 0$ as a function of the photoelectron kinetic energy $E_p - m_e c^2$, for the laser pulse parameters described in Sec. III A. We observe a very broad supercontinuum correlated with the minimum of the imaginary part of $G(g_0,g_1,g_2,h;\phi_s)$ for a particular saddle point (lower panel). $\mathrm{Im}\, G(g_0,g_1,g_2,h;\phi_s)$ for the remaining saddle points are at least two orders of magnitude larger.

also for very short pulses. Therefore, in the remaining part of this paper we shall analyze the process in which the initial and final spins are antiparallel to the propagation direction of the laser pulse. The second dominant process, with the spin projections parallel to the laser field propagation direction, only marginally differs from the first one.

Recently, due to the experimental results reported in Ref. [62] concerning the effects related to the radiation pressure exposed on the atomic or ionic systems by intense laser pulses, we observe an increased interest in theoretical investigations of ionization with the relativistic effects accounted for [47,63–67]. We shall discuss below that the signatures related to the radiation pressure are present in the developed above theoretical approach [cf. our comments below Eq. (26)], although the main focus of our studies is on the formation of a broad ionization supercontinuum.

We consider the probability distribution of electrons $\mathcal{P}_{\downarrow\downarrow}(\boldsymbol{p})$ in a given space direction defined by the polar and azimuthal angles $\theta_p = 0.48\pi$ and $\varphi_p = 0$, respectively. For photoelectron kinetic energies a little bit smaller that 1 keV, which still might be in the domain of applicability of theoretical methods developed above, we observe a typical oscillatory dependence of $\mathcal{P}_{\downarrow\downarrow}(\boldsymbol{p})$ on the energy. This can be interpreted as the interference of probability amplitudes emerging from at least two saddle points. These oscillations, however, gradually disappear with increasing the photoelectron energy. Such that, in the broad part of the spectrum covering few hundreds of the laser carrier frequencies ω_L, we observe a smooth behavior of the probability distribution with the clearly visible maximum for the electron kinetic energy $E_p - m_e c^2 \approx 5565$ eV, as presented in Fig. 2 (upper panel). (For an analysis of the

ionization spectrum over the extended energy interval, see Sec. III F.) As anticipated above, the interpretation of these findings can be based on the analysis of saddle points of the probability amplitude (36). Indeed, in the whole domain, extending from 3 up to 9 keV, there is only one saddle point of imaginary part of $G(g_0,g_1,g_2,h;\phi_s)$ very close to 0, as compared to the remaining saddle points for which $\mathrm{Im}\, G(g_0,g_1,g_2,h;\phi_s)$ are at least two orders of magnitude larger.

The number of laser photons responsible for the formation of supercontinuum presented in Fig. 2 can be estimated from Eq. (28). Namely, using the definition of the laser carrier frequency $\omega_L = N_{\mathrm{osc}}\omega$, we can represent the most probable energy transferred from the pulse to the He^+ ion as

$$E_{\mathrm{tr}} = \frac{N_{\mathrm{eff}}}{N_{\mathrm{osc}}}\omega_L. \tag{46}$$

Hence, the number $N_{\mathrm{eff}}/N_{\mathrm{osc}}$ roughly estimates how many laser photons, each carrying the energy ω_L, have to be absorbed for the photoelectron to be detected with the final energy $E_{\boldsymbol{p}}$. We would like to stress, however, that only for sufficiently long driving pulses this number has a clear interpretation of the order of the multiphoton process, as only in this case the ionization spectrum consists of narrow, well-separated peaks. In the current case, this number ranges from 2030 up to 2430, meaning that the energy region between 2 and 10 keV is covered by 400 laser photons of energy $\omega_L = 20$ eV. Note that, for weak laser fields, only three laser photons of energy $\omega_L = 20$ eV are sufficient to ionize the He^+ ion. On the other hand, for the relativistically intense pulse considered in this paper, around 1930 photons are necessary to liberate the electron. This difference is related to the dressing of the electron by a laser field. One should also remember that, for relativistic fields, this dressing (and the threshold photon number) significantly depends on the emission angles. Hence, in extreme cases such as the Bethe-Heitler process [56,74], the final kinetic energy of electrons is not necessarily an increasing function of the number of absorbed laser photons, which is always the case for the nonrelativistic ionization dynamics.

It has been known since the 1960s (see, for instance, works of Ritus and his collaborators on the fundamental QED processes in the plane wave [75]) that the quiver motion of electrons in the laser field plays the fundamental role in laser-assisted processes. This also concerns the laser-induced ionization of atoms or molecules. The quiver motion is usually quantified by the concept of ponderomotive energy that the electron possesses in the laser field or, equivalently, by the electron effective (or dressed) mass. For nonrelativistic intensities, the effective mass is a marginal modification of the electron rest mass. In this case, the concept of the ponderomotive energy is usually used, the latter being of the order of the laser photon energy. However, for relativistically intense fields, the modification of the effective mass is substantial, and it leads to a significant increase of the energy threshold for ionization. In principle, it is not known how the concept of the effective mass can be generalized to account for very short and intense laser pulses as the ones considered in this paper. However, in our recent works [36,37] we have proposed such generalizations of both the laser-dressed momentum and the electron effective mass in short laser pulses for Compton scattering. If the same can be applied to ionization, the significant increase of the ionization energy threshold can be interpreted (at least qualitatively) as the increase of the electron dressed mass in the laser-dressed final scattering state. Let us note, however, that both concepts, i.e., the ponderomotive energy of the quiver motion and the effective mass, are equivalent, and so the physical interpretations based on them. Let us also stress that the interpretation of the enormous increase of the ionization energy threshold in terms of the electron effective mass in the laser field, although intuitive and plausible, does not account for all aspects of relativistic physics; for instance, contrary to the interpretation based on the most probable energy transferred from the laser pulse (28), it does not explain why the ionization energy threshold depends on the direction of ejected photoelectrons.

Let us analyze further the angular distribution for a particular kinetic energy $E_{\boldsymbol{p}} - m_e c^2 = 5565$ eV, that approximately corresponds to the maximum in the supercontinuum presented in Fig. 2. First, we consider the polar-angle distribution for $\varphi_{\boldsymbol{p}} = 0$. The nonrelativistic theory predicts that, for circularly polarized laser field, ionization occurs predominantly in the plane perpendicular to the direction of propagation. In our case, the maximum of the probability distribution should appear for $\theta_{\boldsymbol{p}} = \pi/2$. However, for sufficiently intense laser pulses, due to the radiation pressure, the maximum should be shifted towards the direction of propagation, i.e., towards smaller angles $\theta_{\boldsymbol{p}}$. This effect is indeed visible as presented in Fig. 3, and can be also attributed to the minimum of $\mathrm{Im}\, G(g_0,g_1,g_2,h;\phi_s)$.

Although the polar-angle distribution of ionization has an expected shape if we account for the laser radiation pressure, the azimuthal angle distribution for relativistic intensities and the high-energy part of the spectrum differ from the predictions of the nonrelativistic SFA. In the nonrelativistic theory for moderately intense laser fields, the ionization occurs with the largest probability when the electric field strength of the laser pulse is maximum (see, e.g., Ref. [19]). Hence, Fig. 1 would suggest that the azimuthal angle distribution should be nearly isotropic. Such pattern is not observed in the relativistic SFA, as presented in Fig. 4. For this particular electron final energy the azimuthal distribution is peaked for $\varphi_{\boldsymbol{p}} = 0.066\pi$ and $\pi - 0.066\pi$. One can interpret this result by performing the saddle-point analysis, presented in Fig. 5. In the lower panel we observe that, for each of the above azimuthal angles, there is one saddle point [we denote it as $\phi_1(\varphi_{\boldsymbol{p}})$] for which the imaginary part of $G(g_0,g_1,g_2,h;\phi_1)$ is very small. It follows from the upper panel of Fig. 5 that these particular azimuthal angles and the real parts of the corresponding saddle points can be grouped in pairs: $[\varphi_{\boldsymbol{p}}, \mathrm{Re}\,\phi_1(\varphi_{\boldsymbol{p}})] = (0.066\pi, 1.68\pi)$ and $(\pi - 0.066\pi, 0.32\pi)$. It is usually assumed that the real parts of the saddle points determine the escape time of electrons from atoms or ions. The values of the electromagnetic vector potential and the electric field strength for these two particular phases $\mathrm{Re}\,\phi_1(\varphi_{\boldsymbol{p}})$ are marked in Fig. 1 by red (dark) open and filled circles. The positions of these points show that the escape of electrons for relativistic intensities takes place not when the electric field strength is maximum (as it is in the nonrelativistic SFA), but for times when the pulse ramps on and off. This happens at least for ions with not very large Z.

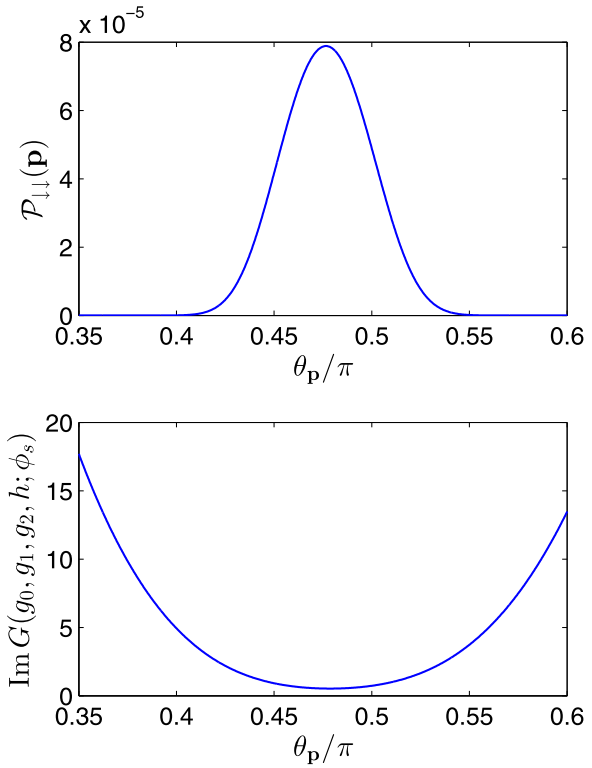

FIG. 3. Upper panel shows the ionization probability $\mathcal{P}_{\downarrow\downarrow}(\boldsymbol{p})$ as a function of θ_p for He^+ ions with energy $E_p - m_e c^2 = 5565$ eV and $\varphi_p = 0$, and for the laser pulse parameters described in Sec. III A. As the result of the radiation pressure, the distribution is shifted towards smaller θ_p angles compared to the expectations based on the nonrelativistic theory. This result agrees with the saddle-point analysis of the probability amplitude (lower panel), where we see that the maximum of the probability amplitude coincides with the minimum of $\mathrm{Im}\, G(g_0,g_1,g_2,h;\phi_s)$.

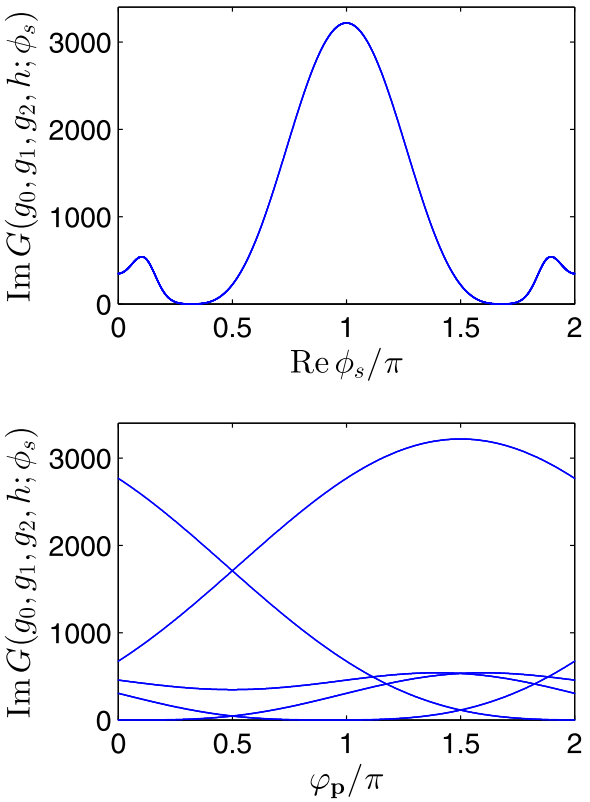

FIG. 5. Shows $\mathrm{Im}\, G(g_0,g_1,g_2,h;\phi_s)$ for $E_p - m_e c^2 = 5565$ eV and $\theta_p = 0.48\pi$. We observe that, for a given azimuthal angle φ_p, there are five saddle points (lower panel). Among them only one, let us say ϕ_1, has a very small positive imaginary part of $G(g_0,g_1,g_2,h;\phi_s)$ which is observed for $\varphi_p = 0.066\pi$ and $\varphi_p = \pi - 0.066\pi$. These values correspond to the real parts of the saddle points $\mathrm{Re}\,\phi_1 = 1.68\pi$ and $\mathrm{Re}\,\phi_1 = 0.32\pi$, respectively, as shown in the upper panel.

C. Azimuthal angle dependence

The width and the position of maximum of the ionization supercontinuum can be controlled by changing the azimuthal angle. It appears that, for the considered laser pulse shape and the azimuthal angle from the upper part of the (x,y) plane, i.e., for $0 < \varphi_p < \pi$, the supercontinuum can be shifted towards lower energies. As a result, the interference pattern starts building up. If, however, we choose φ_p from the interval $(\pi, 2\pi)$, the smooth supercontinuum appears for larger energies. These findings can be also explained by applying the saddle-point analysis.

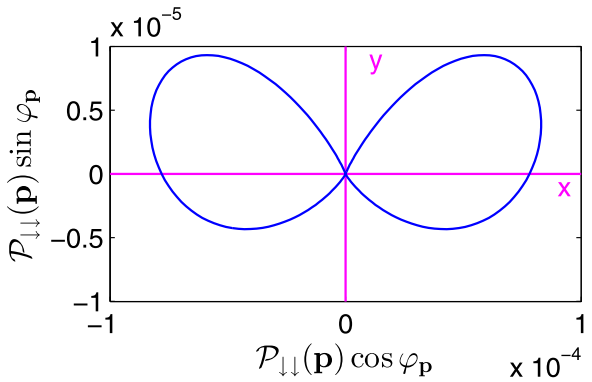

FIG. 4. The ionization probability $\mathcal{P}_{\downarrow\downarrow}(\boldsymbol{p})$ of He^+ ions for $E_p - m_e c^2 = 5565$ eV and $\theta_p = 0.48\pi$ as the function of φ_p, for the laser pulse parameters described in Sec. III A. The vertical scale is much smaller than the horizontal one, meaning that the distribution is tightly elongated around the x direction.

In order to illustrate this effect, let us consider the energy spectrum of photoelectrons ejected in the direction given by spherical angles $\theta_p = 0.48\pi$ and $\varphi_p = 1.8\pi$. This spectrum is presented in the top panel of Fig. 6. We see that now the supercontinuum extends from 8 up to 16 keV with the maximum for $E_p - m_e c^2 \approx 11\,750$ eV. By fixing now the photoelectron kinetic energy $E_p - m_e c^2 = 11\,750$ eV and the polar angle $\theta_p = 0.48\pi$, in the middle panel of Fig. 6 we plot the azimuthal angle distribution of ionization probability. As we see, the side lobes have been turned downwards, but still the symmetry $x \to -x$ is preserved. As in the previous case, we also see the effect of radiation pressure as the maximum of the polar-angle distribution is shifted to the left (the bottom panel of Fig. 6).

In Fig. 7, we present a similar analysis of the imaginary part of $G(g_0,g_1,g_2,h;\phi_s)$ as the function of $\mathrm{Re}\,\phi_s$ (upper panel) and φ_p (lower panel). The minima of this function are

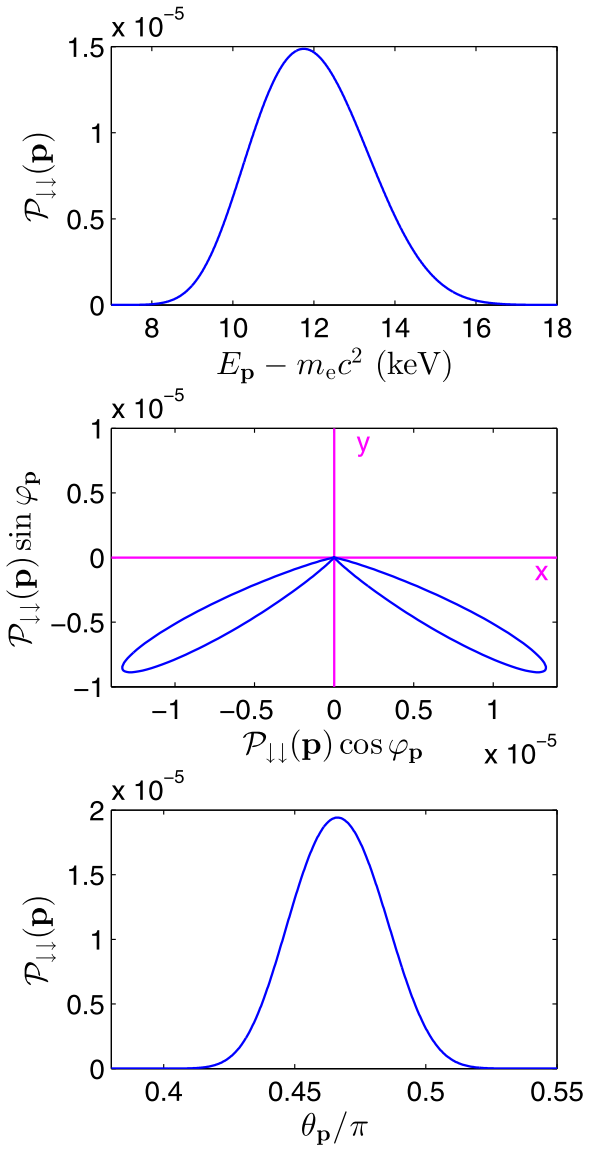

FIG. 6. The same as in Figs. 2, 4, and 3, but respectively for $\theta_p = 0.48\pi$ and $\varphi_p = 1.8\pi$ (top panel), $E_p - m_e c^2 = 11\,750$ eV and $\theta_p = 0.48\pi$ (middle panel), and $E_p - m_e c^2 = 11\,750$ eV and $\varphi_p = 1.8\pi$ (bottom panel).

for $[\varphi_p, \mathrm{Re}\,\phi_1(\varphi_p)] = (1.2\pi, 0.396\pi)$ and $(1.8\pi, 1.604\pi)$, that correspond to cyan (gray) filled and open circles in Fig. 1.

D. Global phase of ionization amplitude

The energy-angular distribution of photoelectrons discussed above depends only on the modulus squared of the probability amplitude $|\mathcal{A}(\boldsymbol{p},\lambda;\lambda_\mathrm{i})|^2$. However, the probability amplitude, as a complex function, is also characterized by the phase $\Phi_\mathcal{A}(\boldsymbol{p},\lambda;\lambda_\mathrm{i})$:

$$\mathcal{A}(\boldsymbol{p},\lambda;\lambda_\mathrm{i}) = \exp[i\,\Phi_\mathcal{A}(\boldsymbol{p},\lambda;\lambda_\mathrm{i})]|\mathcal{A}(\boldsymbol{p},\lambda;\lambda_\mathrm{i})|, \tag{47}$$

$$\Phi_\mathcal{A}(\boldsymbol{p},\lambda;\lambda_\mathrm{i}) = \arg[\mathcal{A}(\boldsymbol{p},\lambda;\lambda_\mathrm{i})], \tag{48}$$

defined up to a constant term not affecting any physically observable quantities. In particular, this constant term

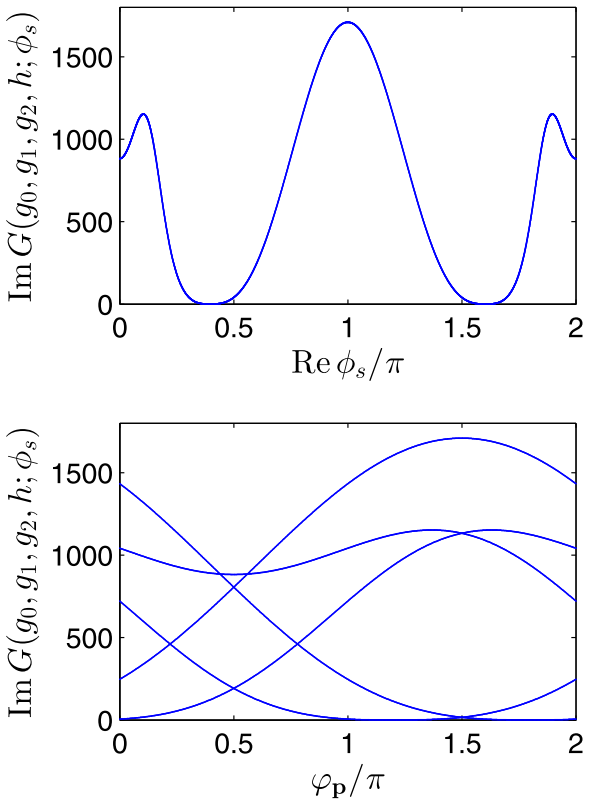

FIG. 7. The same as in Fig. 5, but for $E_p - m_e c^2 = 11\,750$ eV and $\theta_p = 0.48\pi$.

disappears in the derivative of the phase $\Phi_\mathcal{A}$ over the electron energy. This derivative is presented in Fig. 8 for two directions of the electron momentum $\boldsymbol{p}$, for which the azimuthal angular distribution shown in the middle panel of Fig. 6 is maximum, i.e., for the angles (θ_p,φ_p) equal to $(0.48\pi, 1.8\pi)$ and $(0.48\pi, 1.2\pi)$. We see that these derivatives are nearly constant, over a very broad range of electron kinetic energies. This means that the phase $\Phi_\mathcal{A}$ can be well represented for this supercontinuum energy region by the linear dependence

$$\Phi_\mathcal{A}(\boldsymbol{p},\lambda;\lambda_\mathrm{i}) \approx \Phi_0(\boldsymbol{n}_p,\lambda;\lambda_\mathrm{i}) + \Phi_1(\boldsymbol{n}_p,\lambda;\lambda_\mathrm{i})E_p, \tag{49}$$

where $\boldsymbol{n}_p = \boldsymbol{p}/|\boldsymbol{p}|$.

In order to elucidate what are the consequences of this approximate formula, we mention the effects originating from the frequency-dependent phase, similar to (49), in classical and quantum optics. It is known that the space and time dependence of radiation pulses follow from their frequency distributions (see, e.g., [40,76]). For radiation pulses, the constant term Φ_0 does not influence the angular-energy and space-time distributions. On the contrary, the linear term leads to the time delay of pulses; i.e., the larger Φ_1 the larger time delay is observed. This suggests that, as long as Fig. 8 is concerned, the electron wave packet released during ionization in the direction $(\theta_p,\varphi_p) = (0.48\pi, 1.8\pi)$ is delayed with respect to the one propagating in the direction $(\theta_p,\varphi_p) = (0.48\pi, 1.2\pi)$. This is what the above saddle-point analysis predicts, and we are going to address this problem in the next section.

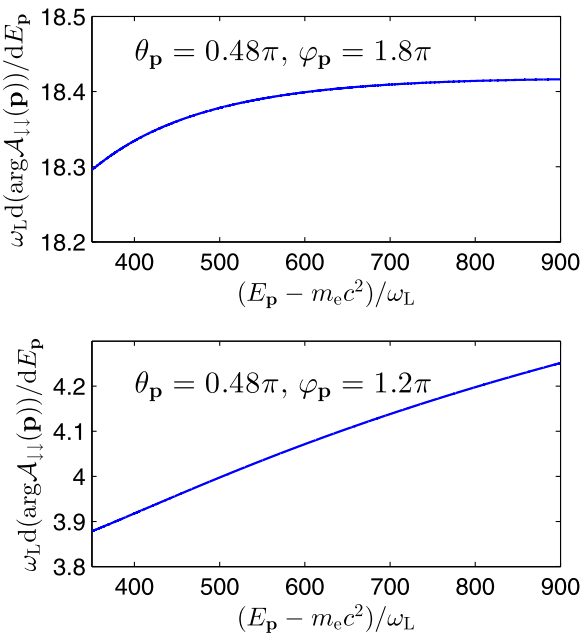

FIG. 8. The derivative of the phase $\Phi_{\mathcal{A}}$ calculated over the electron energy [Eq. (48)] for two directions of emission denoted in each panel. For these angles, the energy distributions are identical and are presented in the upper panel of Fig. 6.

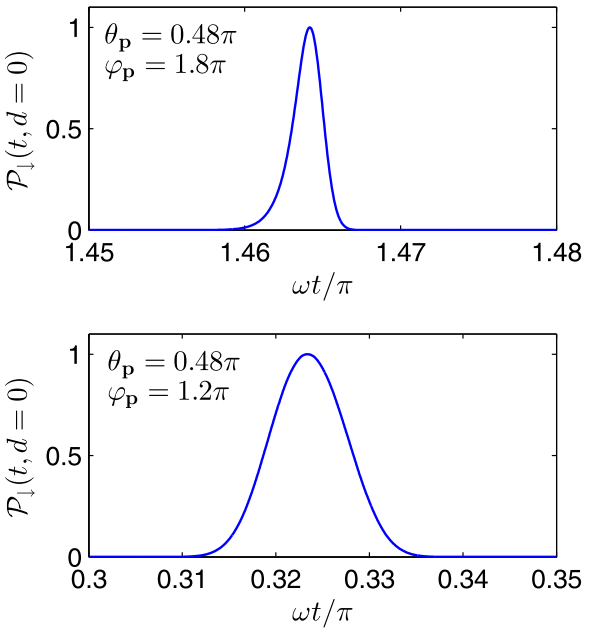

FIG. 9. The normalized probability distribution (53) for electrons escaping in the directions defined by the polar and azimuthal angles as denoted in each panel, and for the remaining parameters same as in Figs. 6 and 8.

E. Space and time analysis

The probability amplitude for the electron to be found at the point x equals

$$\Psi[x,\lambda;\lambda_{\mathrm{i}}|\mathcal{F}] = \int \frac{V d^3p}{(2\pi)^3}\sqrt{\frac{m_e c^2}{V E_p}}\, e^{-ip\cdot x} u^{(+)}_{\boldsymbol{p}\lambda}\mathcal{A}(\boldsymbol{p},\lambda;\lambda_{\mathrm{i}})\mathcal{F}(\boldsymbol{p}). \tag{50}$$

Here, it is assumed that the probability amplitude is calculated for such space-time points x, for which the action of the laser pulse is over, i.e., $A(k\cdot x) = 0$. The so-called filter function $\mathcal{F}(\boldsymbol{p})$ selects only such final electron momenta, from which we are going to build up the wave packet. For our purpose, we select only those electrons that move in a given space direction $\boldsymbol{n}_0$ and have energies from a chosen range. To be more specific, we assume that

$$\begin{aligned}\mathcal{F}(\boldsymbol{p}) = {}& \theta(E_{\max} - E_{\boldsymbol{p}} + m_e c^2)\\ & \times \theta(E_{\boldsymbol{p}} - m_e c^2 - E_{\min})\delta^{(2)}(\Omega_{\boldsymbol{p}} - \Omega_{\boldsymbol{n}_0}),\end{aligned} \tag{51}$$

where $\theta(E)$ is the Heaviside step function, $E_{\min} = 7$ keV, and $E_{\max} = 18$ keV (cf. the top panel of Fig. 6). Hence, the electron wave packet propagating in the space direction $\boldsymbol{x} = d\boldsymbol{n}_0$ (where d is the distance from the nucleus), and with initial and final spins antiparallel to the laser pulse propagation direction, is proportional to

$$\begin{aligned}\mathcal{A}_{\downarrow}(t,d) \sim {}& \int_{E_{\min}+m_e c^2}^{E_{\max}+m_e c^2} dE_{\boldsymbol{p}}\, e^{-iE_{\boldsymbol{p}}t + i|\boldsymbol{p}|d} u^{(+)}_{|\boldsymbol{p}|\boldsymbol{n}_0,\downarrow}\\ & \times \sqrt{E_{\boldsymbol{p}}}\,|\boldsymbol{p}|\mathcal{A}(|\boldsymbol{p}|\boldsymbol{n}_0,\downarrow;\downarrow),\end{aligned} \tag{52}$$

where we have neglected all irrelevant prefactors. Finally, the time-distance probability distribution of these selected electrons is equal to

$$\mathcal{P}_{\downarrow}(t,d) = [\mathcal{A}_{\downarrow}(t,d)]^{\dagger}\mathcal{A}_{\downarrow}(t,d). \tag{53}$$

Although the last definition applies to positive times t and distances d such that $k\cdot x = \omega t - (\omega/c)d\boldsymbol{n}\cdot\boldsymbol{n}_0 > 2\pi$, nevertheless, by extrapolating its validity to $d = 0$ (where the nucleus is located) we can roughly estimate the escape time from the ion of the selected electrons, as it is presented in Fig. 9. We can judge from the positions of maxima that the escape times for the selected group of photoelectrons are around $\omega t = 1.464\pi$ for the direction $(\theta_{\boldsymbol{p}},\varphi_{\boldsymbol{p}}) = (0.48\pi, 1.8\pi)$ and $\omega t = 0.323\pi$ for the direction $(\theta_{\boldsymbol{p}},\varphi_{\boldsymbol{p}}) = (0.48\pi, 1.2\pi)$. This agrees reasonably well with the predictions based on the saddle-point analysis, where we have estimated these times to be $\omega t = \mathrm{Re}\,\phi_1 = 1.604\pi$ and $\omega t = \mathrm{Re}\,\phi_1 = 0.396\pi$, respectively.

The widths of the distributions presented in Fig. 9 are not larger than 10^{-2}. This means that, at the time of escape, electrons from these supercontinua are created in very short pulses lasting for

$$\Delta t \approx 10^{-2}\pi\frac{1}{\omega} = \frac{10^{-2}\pi}{5\ \mathrm{eV}/\hbar} \approx 10^{-17}\ \mathrm{s}. \tag{54}$$

Then, during the time evolution, the electron wave packets spread. However, even at the distance $5000a_0$ from the ion their time durations are of the order of 10^{-15} s, as it is shown in Fig. 10. As expected, the pulses presented there are delayed with respect to each other by the time approximately equal to $1.15\pi/\omega$. This quite well agrees with predictions of the Keldysh theory.

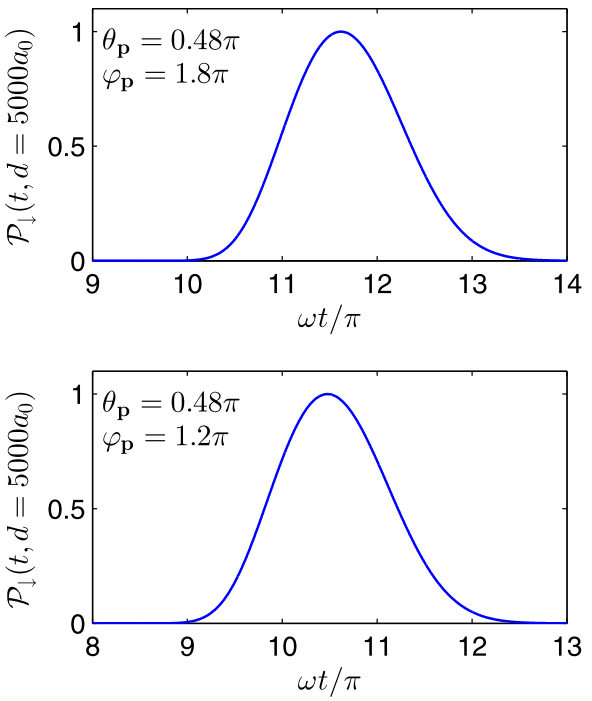

FIG. 10. The same as in Fig. 9 but for the distance $d = 5000a_0$ from the nucleus, where a_0 is the Bohr radius.

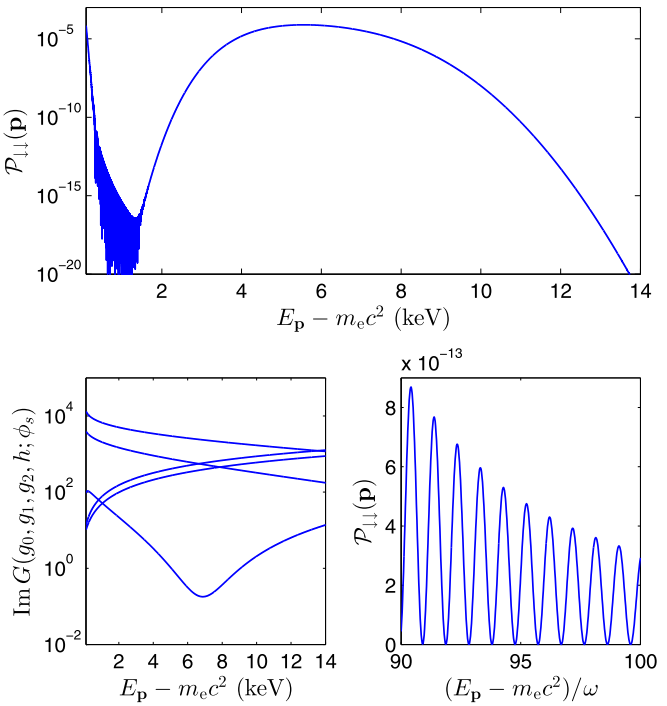

FIG. 11. The same as in Fig. 2 but this time the upper panel shows the probability distribution $\mathcal{P}_{\downarrow\downarrow}(\boldsymbol{p})$ in the logarithmic scale and for the broader energy region. In the lower left panel, we demonstrate the dependence of $\mathrm{Im}G(g_0, g_1, g_2, h; \phi_s)$ on the electron kinetic energy for five relevant saddle points. In the lower right panel, the probability distribution is presented for electron energies between 450 and 500 eV, where the interference effects are significant. As we see, the peaks in the spectrum are separated by roughly the fundamental laser frequency ω, which is related to the time duration of the short pulse (not by the laser carrier frequency ω_L, which is the case for long pulses).

F. Low- and high-energy structures

Our focus so far has been on the high-energy portion of the photoelectron ionization spectrum. This is justified because, in our theoretical approach, we have applied the Born approximation in the final scattering state of the electron. Note that, since the Born approximation is in general valid for high energies, the presented theoretical method can provide only a qualitative insight into the low-energy portion of the electron spectrum. For this reason, the Monte Carlo evaluation of the total probability of ionization (29), presented in Appendix D, can be only considered as an estimation. Having this in mind, we analyze below the ionization probability distributions $\mathcal{P}_{\downarrow\downarrow}(\boldsymbol{p})$ starting from nearly the ionization threshold up to the high-energy domain of photoelectrons.

In the upper panel of Fig. 11, we demonstrate the ionization spectrum of photoelectrons (in the logarithmic scale) for the same parameters as in Fig. 2 but over a wider interval of the electron kinetic energies. It is clearly seen that the spectrum changes its behavior for electron kinetic energies around 1 keV; while for smaller energies the spectrum exhibits the interference pattern, the pattern disappears otherwise. Instead, in the high-energy region of the spectrum, we see a smooth and very broad supercontinuum. As we have already anticipated, the theoretical interpretation of this different behavior can be based on the saddle-point analysis of the probability amplitude (cf. Sec. II C). For this reason, in the lower left panel of Fig. 11, we plot the energy dependence of $\mathrm{Im}G(g_0, g_1, g_2, h; \phi_s)$ for all relevant saddle points. These points were defined in Sec. III B such that $\mathrm{Im}G(g_0, g_1, g_2, h; \phi_s) > 0$. As it is clearly demonstrated, for energies smaller than 1 keV there are two saddle points with comparable, but much smaller than other, values of $\mathrm{Im}G(g_0, g_1, g_2, h; \phi_s)$. The contributions to the probability amplitude of ionization coming from these two dominant saddle points result in interference. For larger energies, $\mathrm{Im}G(g_0, g_1, g_2, h; \phi_s)$ for a particular saddle point departs from the others, reaches the minimum at around 7 keV (cf. Fig. 2), and then increases. Exactly for these energies the ionization supercontinuum is formed. The same does not occur if the driving pulse is linearly polarized. In this case, as we demonstrate in Appendix A, the probability distributions $\mathcal{P}_{\downarrow\downarrow}(\boldsymbol{p})$ always exhibit very pronounced interferences.

In the lower right panel of Fig. 11, we plot (in the linear scale) the enlarged portion of the distribution from the interference-dominated low-energy region. We clearly see the so-called multiphoton peaks approximately separated by the fundamental frequency $\omega = \omega_L/N_{\mathrm{osc}} = 5$ eV. This is in contrast to the very long pulses, for which the peaks are separated by the laser carrier frequency ω_L. The reason for this difference is that, for very short laser pulses, the Fourier decomposition of the electric field shows components of comparable strength for integer multiples of ω. On the contrary, for long pulses, only one component corresponding to the carrier frequency dominates in the Fourier decomposition of the pulse. This pattern is preserved for shorter and longer pulses, with $N_{\mathrm{osc}} = 3$ and 5, correspondingly, as it is discussed below.

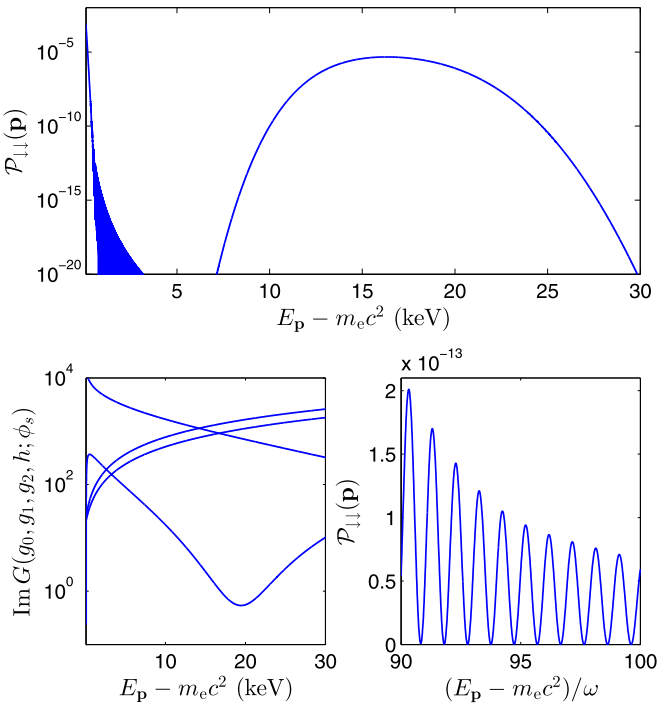

FIG. 12. The same as in Fig. 11 but for the shorter pulse, with $N_{\mathrm{osc}} = 3$. The probability distribution in the upper panel is shown starting with values of the order of 10^{-20}, which is the accuracy of our numerical calculations. For $N_{\mathrm{osc}} = 3$, there are only four relevant saddle points, i.e., the ones with the positive $\mathrm{Im}G(g_0, g_1, g_2, h; \phi_s)$.

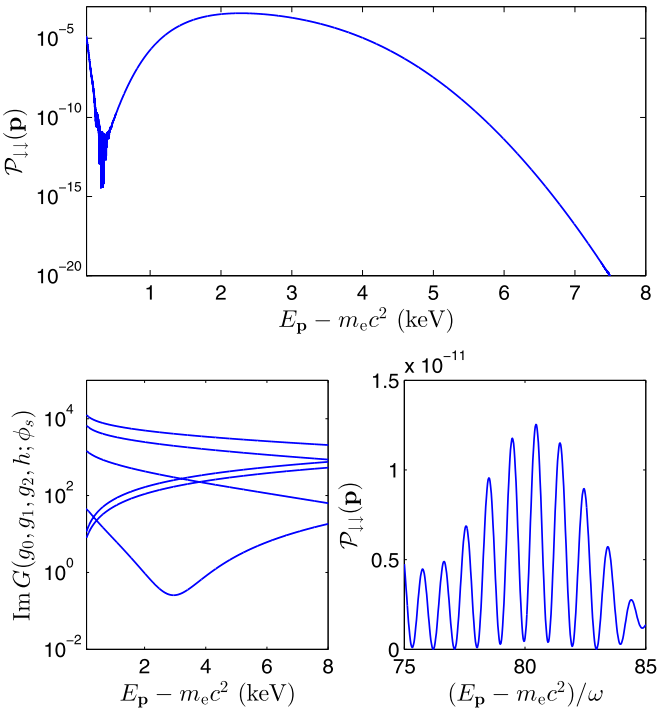

FIG. 13. The same as in Fig. 11 but for the longer pulse, with $N_{\mathrm{osc}} = 5$, and six relevant saddle points.

G. Ionization by shorter versus longer pulses

If the averaged intensity and the carrier frequency of the laser pulse are fixed, the time-averaged ponderomotive energy of the electron moving in the pulse [Eq. (45)] is a decreasing function of N_{osc} (see Appendix C). We expect, therefore, that, under such constraints, more laser photons have to be absorbed from shorter pulses in order to liberate electrons from atoms or ions. This indicates that the ionization spectrum, and, specifically, the properties of the supercontinuum, will crucially depend on the pulse duration. In order to study this effect, we will compare now the probability distributions of ionization by a three-cycle ($N_{\mathrm{osc}} = 3$) and a five-cycle ($N_{\mathrm{osc}} = 5$) driving pulse.

Figure 12 shows the results for the three-cycle pulse, $N_{\mathrm{osc}} = 3$, with the time-averaged intensity and laser carrier frequency same as for the four-cycle pulse $N_{\mathrm{osc}} = 4$ studied so far. It follows from Eq. (28) that, in the current case, the minimum number of photons carrying the energy $\omega_L = 20$ eV, which are required to ionize the H_2^+ ion, is around 2050, as compared to 1930 for $N_{\mathrm{osc}} = 4$. As above, we clearly see the separation of the probability distribution into the interference-dominated low-energy region and the smooth and even broader high-energy supercontinuum. Note that, this time, the maximum of the supercontinuum is shifted toward higher electron kinetic energies and appears at roughly 16 keV. This shift can be interpreted as the result of a larger ponderomotive acceleration experienced by electrons leaving the focus of a shorter pulse. This follows from the fact that, under current conditions, the ponderomotive energy is a decreasing function of N_{osc} and, hence, its gradient is larger for shorter pulses. Rather than that, the qualitative picture we have gained from the analysis performed for $N_{\mathrm{osc}} = 4$ is not changed.

The same conclusions can be reached when studying ionization of the He^+ ion by the five-cycle pulse $N_{\mathrm{osc}} = 5$, as presented in Fig. 13. As anticipated, the high-energy portion of the spectrum is now shifted toward smaller electron kinetic energies. We also observe that the energy region which separates the low- and high-energy portions of the distribution has shrunk. Thus, one could expect that, for still longer pulses, the two portions of the spectrum merge into one and the interference pattern gets reestablished, at least partially. Such investigations are, however, beyond the scope of this paper which focuses on the interference-free supercontinuum in the high-energy region of the ionization spectrum.

In closing this section let us mention the results presented in Ref. [48], where the relativistic ionization by a circularly polarized monochromatic plane wave was discussed in connection with the stabilization problem. The ionization rates calculated there show seemingly broad structures in the high-energy portion of the spectrum. However, these structures are composed of discrete points. For a finite but very long pulse with a flat-top envelope, such points represent very narrow peaks which can be attributed to the so-called intercycle and intracycle interferences [4–6,35]. In the limit of infinitely long and, in general, multichromatic plane wave (when there are infinitely many saddle points equally contributing to the probability amplitude) these peaks are represented by the δ functions. Therefore, the results presented in [48] cannot be related to the supercontinuum discussed in this paper, which appears only for very short pulses and in the energy and angular

domains where there is only one dominant complex-time saddle point.

IV. CONCLUSIONS

We have developed the theoretical formulation for relativistic ionization driven by an arbitrary laser pulse. This has been done in the velocity gauge, within the lowest-order Born approximation with respect to the atomic potential. As an illustration, we have studied ionization of He^+ by a short, relativistically intense, circularly polarized pulse. As our analysis shows, it is possible to adjust parameters of the pulse and the target system such that high-order nonlinear processes result in appearance of a broad supercontinuum in the energy spectrum of photoelectrons.

We have further analyzed the properties of supercontinuum electrons. We have checked that they are predominantly ionized through the spin-conserved processes. We have also observed that, in contrast to the nonrelativistic ionization by circularly polarized pulses, the polar-angle distributions of photoelectrons are asymmetric. This has been ascribed to the radiation pressure experienced by electrons. As we have argued, in the energy region of supercontinuum, the total phase of the probability amplitude of ionization can be approximated as a linear function of the photoelectron energy. Therefore, the electron pulses composed out of this part of the spectrum can be delayed with respect to each other. More importantly, the supercontinuum electrons can form very short pulses. Despite the fact that they are spreading in time, we have demonstrated that these pulses remain fairly short.

We have shown numerically that relativistic ionization can lead to the formation of electron supercontinua. This is particularly interesting in the context of designing new sources of electron pulses. While our analysis is based on purely numerical treatment, we have also performed an analysis of probability amplitudes based on approximation via the saddle-point method. The latter has shown, for instance, that relativistic ionization can occur with significant probabilities at the pedestal of the driving pulse, not, like in nonrelativistic ionization, at the pulse maximum. It has also shown that the ionization supercontinua are highly sensitive to the duration and polarization of the driving pulse. Other predictions of the saddle-point approximation have also agreed well with our fully numerical results.

ACKNOWLEDGMENTS

This work is supported by the National Science Centre (Poland) under Grant No. 2014/15/B/ST2/02203. K.K. also acknowledges the support from the Kosciuszko Foundation. We would like to thank Professor S. Bhattacharyya for discussions.

APPENDIX A: LINEARLY POLARIZED PULSES

The main focus of our investigations has been on the formation of supercontinuum in the high-energy portion of the ionization probability distribution. In this context, it is essential that the driving pulse is circularly polarized and short. However, for the completeness of our discussion, we present here the results for a linearly polarized pulse. As we demonstrate in Fig. 14, in this case one cannot expect the creation of supercontinuum. The reason being that, for the linearly polarized pulse, there are at least two saddle points corresponding to small values of $\mathrm{Im}G(g_0,g_1,g_2,h;\phi_s)$, which lead to interference of the contributing probability amplitudes. Moreover, for the very short and relativistically intense laser pulse considered in this Appendix, the interferences lead to the peak structure. The latter is clearly unrelated to the fundamental or to the laser carrier frequency. The investigation of this problem is beyond the scope of this paper.

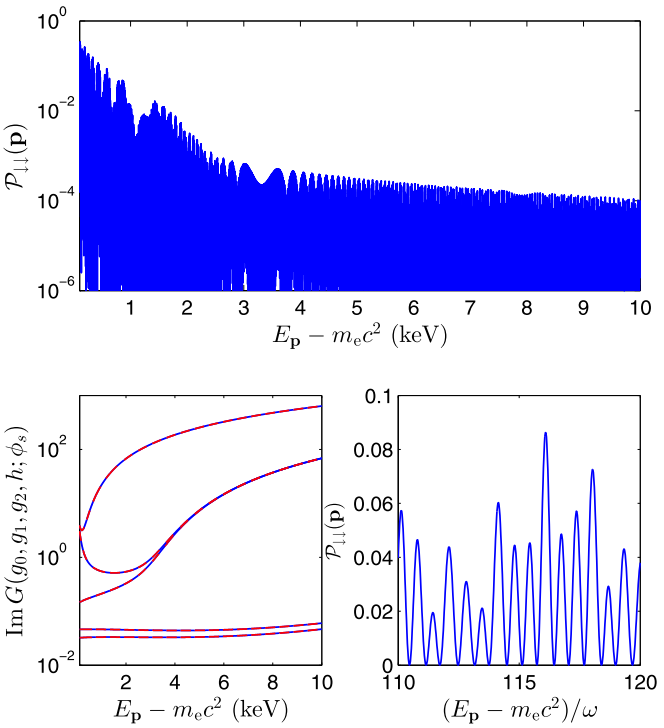

FIG. 14. The same as in Fig. 11 but for the laser pulse linearly polarized along the x axis. Note that in this case there are 10 relevant saddle points grouped in pairs of the same $\mathrm{Im}G(g_0,g_1,g_2,h;\phi_s)$. That is why a given curve in the lower left panel represents two curves (solid blue and dashed red). Due to this property, the interference pattern is present over the whole energy domain (upper panel) and the separation of peaks (lower right panel) is not related to the fundamental laser frequency ω, which should be the case for such short pulse.

APPENDIX B: REMARKS ON PHYSICAL UNITS

The time-averaged intensity of a pulse described in the plane-wave front approximation equals

$$I = \left(\left\langle f_1'^2\right\rangle + \left\langle f_2'^2\right\rangle\right)\varepsilon_0 c\frac{(\omega m_e c)^2}{e^2}\mu^2, \tag{B1}$$

where ω is related to the pulse duration T_p such that $T_p = 2\pi/\omega$. If the number of cycles is N_{osc} then the carrier frequency is $\omega_L = N_{\mathrm{osc}}\omega$, and in our analysis we keep it fixed. In order to have the time-averaged intensity independent of the number of cycles in the pulse we choose the normalization of the shape

functions such that

$$\langle f_1'^2\rangle + \langle f_2'^2\rangle = \tfrac{1}{2}N_{\rm osc}^2 \tag{B2}$$

and, consequently,

$$I = \frac{1}{2}\varepsilon_0 c\frac{(\omega_L m_e c)^2}{e^2}\mu^2. \tag{B3}$$

We can rewrite this relation as

$$I = I_{\rm rel}\left(\frac{\hbar\omega_L}{m_e c^2}\right)^2\mu^2, \tag{B4}$$

where we have restored the Planck constant $\hbar$, and where $I_{\rm rel}$ is the relativistic unit of intensity

$$I_{\rm rel} = \frac{m_e c^3}{8\pi\alpha\lambda\!\!\!^{-3}_C} = \frac{m_e^4 c^6}{8\pi\alpha\hbar^3} \approx 2.324\times10^{29}\ {\rm W/cm^2}. \tag{B5}$$

Here, $\lambda\!\!\!^{-}_C = \hbar/m_e c$ is the Compton wavelength divided by 2π. On the other hand, the nonrelativistic unit of intensity is equal to

$$I_{\rm nrel} = \alpha^6 I_{\rm rel} \approx 3.51\times10^{16}\ {\rm W/cm^2}. \tag{B6}$$

Thus,

$$I = I_{\rm nrel}\left(\frac{\hbar\omega_L}{\alpha^2 m_e c^2}\right)^2\mu_{\rm nrel}^2, \tag{B7}$$

where $\alpha^2 m_e c^2 \approx 27.21$ eV is the nonrelativistic unit of energy and

$$\mu_{\rm nrel} = \frac{\mu}{\alpha} = \frac{|eA_0|}{\alpha m_e c}. \tag{B8}$$

Above, $\alpha m_e c = \hbar/a_0$ is the nonrelativistic unit of momentum and a_0 is the Bohr radius.

Equations (B4) and (B7) allow one to relate the parameter μ in (8) to the time-averaged intensity of the laser pulse given in the standard units of W/cm^2.

APPENDIX C: REMARKS ON SINE-SQUARED CIRCULARLY POLARIZED PULSE

For a sine-squared circularly polarized pulse, defined in the beginning of Sec. III A, we choose in Eq. (42)

$$N_0 = \sqrt{\frac{8}{3}}\,N_{\rm osc}. \tag{C1}$$

With this choice, the time-averaged intensity of the pulse I [Eq. (B1)] is independent of the number of cycles, i.e., the condition (B2) is satisfied. Now, let us assume that the pulse peak intensity $I_{\rm max}$ is the intensity of the circularly polarized plane wave, which is defined by Eq. (42) with the envelope function $\sin^2(\phi/2)$ replaced by 1. In this case,

$$I_{\rm max} = \tfrac{8}{3}\,I, \tag{C2}$$

showing that $I_{\rm max}$ does not depend on the number of cycles in the pulse either.

Calculating now the time-averaged ponderomotive energy (45), we obtain

$$U = \tfrac{1}{2}m_e c^2\mu^2 g(N_{\rm osc}), \tag{C3}$$

where

$$g(N_{\rm osc}) = \frac{1}{3}\left\{1+\left[\frac{N_{\rm osc}}{2(N_{\rm osc}-1)}\right]^2+\left[\frac{N_{\rm osc}}{2(N_{\rm osc}+1)}\right]^2\right\}. \tag{C4}$$

Hence, one concludes that, for the pulse under considerations, the time-averaged ponderomotive energy (C3) decreases with increasing the number of pulse cycles. Note also that, in the limit of very large $N_{\rm osc}$, we obtain the well-known expression for the ponderomotive energy of a plane wave

$$U = \tfrac{1}{4}m_e c^2\mu^2 = \tfrac{1}{4}\alpha^2 m_e c^2\mu_{\rm nrel}^2. \tag{C5}$$

APPENDIX D: TOTAL IONIZATION PROBABILITY

The total probability of ionization by circularly polarized pulses is defined by the three-dimensional integral

$$P_{\rm ion} = \int_0^{2\pi} d\varphi_{\boldsymbol{p}} \int_{-1}^{1} d\cos\theta_{\boldsymbol{p}} \int_{m_e c^2}^{\infty} dE_{\boldsymbol{p}}\, F(\boldsymbol{p}), \tag{D1}$$

where [cf. Eqs. (29) and (30)]

$$F(\boldsymbol{p}) = \frac{1}{2}\sum_{\lambda,\lambda_{\rm i}=\pm}\frac{d^3P(\boldsymbol{p},\lambda;\lambda_{\rm i})}{dE_{\boldsymbol{p}}d^2\Omega_{\boldsymbol{p}}}, \tag{D2}$$

and where the factor $\frac{1}{2}$ is due to the initial spin averaging. In order to evaluate this integral, we perform the Monte Carlo analysis (see, e.g., Refs. [28,77]). To this end, we replace the upper limit of the energy integration by a finite value $m_e c^2 + E_{\rm max}$, with $E_{\rm max}$ being the maximum kinetic energy of ejected electrons. We put $E_{\rm max} = 30$ keV as, for laser pulse intensities considered in this paper, the triply differential probability distribution (30) is marginally small for kinetic energies larger than 30 keV. Next, changing the integration variables ($0 < \xi_i < 1$, $i = 1,2,3$) such that

$$\varphi_{\boldsymbol{p}} = 2\pi\xi_1, \quad \cos\theta_{\boldsymbol{p}} = 2\xi_2 - 1, \quad E_{\boldsymbol{p}} = m_e c^2 + E_{\rm max}\xi_3, \tag{D3}$$

we arrive at the three-dimensional integral over the unit cube

$$P_{\rm ion} = \int_0^1 d\xi_1 d\xi_2 d\xi_3\, 4\pi\, E_{\rm max} F(\boldsymbol{p}). \tag{D4}$$

This integral is estimated using the Monte Carlo integration with the uniformly distributed ξ_i.

The estimated values for $P_{\rm ion}$ are 0.44, 0.36, and 0.3 for $N_{\rm osc} = 3$, 4, and 5, respectively. These numbers are based on the evaluation of not less then 10^6 sample points with the estimated relative standard deviations smaller than 3%. Note that the total probability of ionization decreases with increasing the number of cycles in a pulse. A more elaborate Monte Carlo analysis is under investigations and is going to be presented in due course.

[1] L. V. Keldysh, Zh. Eksp. Teor. Fiz. **47**, 1945 (1964) [Sov. Phys. JETP **20**, 1307 (1965)].

[2] A. M. Perelomov, V. S. Popov, and M. V. Terent'ev, Zh. Eksp. Teor. Fiz. **50**, 1393 (1966) [Sov. Phys. JETP **23**, 924 (1966)].

[3] G. F. Gribakin and M. Yu. Kuchiev, Phys. Rev. A **55**, 3760 (1997).

[4] D. G. Arbó, K. L. Ishikawa, K. Schiessl, E. Persson, and J. Burgdörfer, Phys. Rev. A **82**, 043426 (2010).

[5] D. G. Arbó, S. Nagele, X.-M. Tong, X. Xie, M. Kitzler, and J. Burgdörfer, Phys. Rev. A **89**, 043414 (2014).

[6] D. G. Arbó, J. Phys. B: At., Mol. Opt. Phys. **47**, 204008 (2014).

[7] Gy. Farkas and Cs. Tóth, Phys. Lett. A **168**, 447 (1992).

[8] P. Agostini and L. F. DiMauro, Rep. Prog. Phys. **67**, 813 (2004).

[9] D. B. Milošević, G. G. Paulus, D. Bauer, and W. Becker, J. Phys. B: At., Mol. Opt. Phys. **39**, R203 (2006).

[10] F. Krausz and M. Ivanov, Rev. Mod. Phys. **81**, 163 (2009).

[11] P. Salières, A. Maquet, S. Haessler, J. Caillat, and R. Taïeb, Rep. Prog. Phys. **75**, 062401 (2012).

[12] J. M. Dahlström, A. L'Huillier, and A. Maquet, J. Phys. B: At., Mol. Opt. Phys. **45**, 183001 (2012).

[13] B. M. Karnakov, V. D. Mur, S. V. Popruzhenko, and V. S. Popov, Phys. Usp. **58**, 3 (2015).

[14] Special issue on 50 years of optical tunneling: J. Phys. B: At., Mol. Opt. Phys. 47, issue 20 (2014).

[15] The routinely used Keldysh theory [1] provides the ansatz for the transition matrix element of ionization by an intense radiation field leading, after the saddle-point analysis is performed, to the tunneling formula. Hence, it is considered as the tunneling theory of ionization. However, one can understand the Keldysh theory within a more general framework, as it has initiated the use of the saddle-point method in strong-field physics. Specifically, in the original work of Keldysh [1] and in the subsequent studies (see, e.g., [14]) the concepts of the complex time and the complex-time trajectories have been put forward. These concepts are used in this paper to provide a physical interpretation of our numerical results. For this reason, we place our investigations within a general framework of the Keldysh approach to photoionization by intense laser fields. We would like to stress, however, that in our studies we use the Born approximation for the scattering state of photoelectrons (which proved its validity for kinetic energies of photoelectrons much larger than the ionization potential of atoms or ions), and that the remaining transition matrix element is analyzed numerically without further approximations.

[16] V. S. Popov, Phys. Usp. **47**, 855 (2004).

[17] V. S. Popov, Phys. At. Nucl. **68**, 686 (2005).

[18] S. V. Popruzhenko, J. Phys. B: At., Mol. Opt. Phys. **47**, 204001 (2014).

[19] F. Cajiao Vélez, K. Krajewska, and J. Z. Kamiński, Phys. Rev. A **91**, 053417 (2015).

[20] F. H. M. Faisal, J. Phys. B: At. Mol. Phys. **6**, L89 (1973).

[21] H. R. Reiss, Phys. Rev. A **22**, 1786 (1980).

[22] F. Ehlotzky, K. Krajewska, and J. Z. Kamiński, Rep. Prog. Phys. **72**, 046401 (2009).

[23] A. Di Piazza, C. Müller, K. Z. Hatsagortsyan, and C. H. Keitel, Rev. Mod. Phys. **84**, 1177 (2012).

[24] S. P. Roshchupkin, A. A. Lebed', E. A. Padusenko, and A. I. Voroshilo, Laser Phys. **22**, 1113 (2012).

[25] B. King, A. Di Piazza, and C. H. Keitel, Nat. Photon. **4**, 92 (2010).

[26] S. Ahrens, H. Bauke, C. H. Keitel, and C. Müller, Phys. Rev. Lett. **109**, 043601 (2012).

[27] M. M. Dellweg and C. Müller, Phys. Rev. A **91**, 062102 (2015).

[28] K. Krajewska and J. Z. Kamiński, Phys. Rev. A **90**, 052117 (2014).

[29] T. N. Wistisen, Phys. Rev. D **90**, 125008 (2014); **91**, 069903(E) (2015).

[30] S. P. Roshchupkin and A. A. Lebed', Phys. Rev. A **90**, 035403 (2014).

[31] A. A. Lebed', Laser Phys. **25**, 055301 (2015); Laser Phys. Lett. **13**, 045401 (2016).

[32] K. Krajewska and J. Z. Kamiński, Laser Phys. Lett. **11**, 035301 (2014).

[33] K. Krajewska, M. Twardy, and J. Z. Kamiński, Phys. Rev. A **89**, 052123 (2014).

[34] K. Krajewska and J. Z. Kamiński, Phys. Rev. A **90**, 052108 (2014).

[35] K. Krajewska and J. Z. Kamiński, Phys. Lett. A **380**, 1247 (2016).

[36] K. Krajewska, F. Cajiao Vélez, and J. Z. Kamiński, Phys. Rev. A **91**, 062106 (2015).

[37] F. Cajiao Vélez, K. Krajewska, and J. Z. Kamiński, J. Phys. Conf. Ser. **691**, 012005 (2016).

[38] R. R. Alfano and S. L. Shapiro, Phys. Rev. Lett. **24**, 584 (1970); **24**, 592 (1970).

[39] J. M. Dudley, G. Genty, and S. Coen, Rev. Mod. Phys. **78**, 1135 (2006).

[40] K. Krajewska, M. Twardy, and J. Z. Kamiński, Phys. Rev. A **89**, 032125 (2014).

[41] M. Kalashnikov, A. Andreev, K. Ivanov, A. Galkin, V. Korobkin, M. Romanovsky, O. Shiryaev, M. Schnuerer, J. Braenzen, and V. Trofimov, Laser Part. Beams **33**, 361 (2015).

[42] www.eli-laser.eu

[43] S. Selstø, E. Lindroth, and J. Bengtsson, Phys. Rev. A **79**, 043418 (2009).

[44] H. Bauke and C. H. Keitel, Comput. Phys. Commun. **182**, 2454 (2011).

[45] Y. V. Vanne and A. Saenz, Phys. Rev. A **85**, 033411 (2012).

[46] R. Beerwerth and H. Bauke, Comput. Phys. Commun. **188**, 189 (2015).

[47] I. A. Ivanov, Phys. Rev. A **91**, 043410 (2015).

[48] D. P. Crawford and H. R. Reiss, Phys. Rev. A **50**, 1844 (1994).

[49] F. H. M. Faisal and S. Bhattacharyya, Phys. Rev. Lett. **93**, 053002 (2004).

[50] F. H. M. Faisal and S. Bhattacharyya, in *Progress in Ultrafast Intense Laser Science VII*, edited by K. Yamanouchi, D. Charalambidis and D. Normand, Springer Series in Chemical Physics (Springer, Berlin, 2011), Vol. 100, p. 1.

[51] M. Klaiber, E. Yakaboylu, and K. Z. Hatsagortsyan, Phys. Rev. A **87**, 023418 (2013).

[52] M. Klaiber and K. Z. Hatsagortsyan, Phys. Rev. A **90**, 063416 (2014).

[53] E. Yakaboylu, M. Klaiber, and K. Z. Hatsagortsyan, Phys. Rev. A **91**, 063407 (2015).

[54] K. Lee, S. Y. Chung, S. H. Park, Y. U. Jeong, and D. Kim, Europhys. Lett. **89**, 64006 (2010).

[55] D. M. Wolkow, Z. Phys. **94**, 250 (1935).

[56] K. Krajewska and J. Z. Kamiński, Phys. Rev. A **82**, 013420 (2010).

[57] J. D. Bjorken and S. D. Drell, *Relativistic Qauntum Mechanics* (McGraw-Hill, New York, 1964).
[58] K. Krajewska and J. Z. Kamiński, Phys. Rev. A **85**, 062102 (2012).
[59] K. Krajewska and J. Z. Kamiński, Phys. Rev. A **86**, 052104 (2012).
[60] K. Krajewska, C. Müller, and J. Z. Kamiński, Phys. Rev. A **87**, 062107 (2013).
[61] P. Lebedew, Ann. Phys. **311**, 433 (1901).
[62] C. T. L. Smeenk, L. Arissian, B. Zhou, A. Mysyrowicz, D. M. Villeneuve, A. Staudte, and P. B. Corkum, Phys. Rev. Lett. **106**, 193002 (2011).
[63] A. S. Titi and G. W. F. Drake, Phys. Rev. A **85**, 041404(R) (2012).
[64] H. R. Reiss, Phys. Rev. A **87**, 033421 (2013).
[65] S. Chelkowski, A. D. Bandrauk, and P. B. Corkum, Phys. Rev. Lett. **113**, 263005 (2014); Phys. Rev. A **92**, 051401(R) (2015).
[66] M. Førre and A. S. Simonsen, Phys. Rev. A **90**, 053411 (2014).
[67] K. Krajewska and J. Z. Kamiński, Phys. Rev. A **92**, 043419 (2015).
[68] C. Müller, A. B. Voitkiv, and N. Grün, Phys. Rev. Lett. **91**, 223601 (2003).
[69] M. Yabashi *et al.*, J. Phys. B: At., Mol. Opt. Phys. **46**, 164001 (2013).
[70] J. Feldhaus *et al.*, J. Phys. B: At., Mol. Opt. Phys. **46**, 164002 (2013).
[71] C. Bostedt *et al.*, J. Phys. B: At., Mol. Opt. Phys. **46**, 164003 (2013).
[72] F. Sauter, Z. Phys. **69**, 742 (1931).
[73] J. Schwinger, Phys. Rev. **82**, 664 (1951).
[74] K. Krajewska, Laser Phys. **21**, 1275 (2011).
[75] V. I. Ritus, J. Sov. Laser Res. **6**, 497 (1985).
[76] R. Trebino, *Frequency-Resolved Optical Gating: The Measurement of Ultrashort Laser Pulses* (Kluwer Academic, Boston, 2000).
[77] J. Z. Kamiński, K. Krajewska, and F. Ehlotzky, Phys. Rev. A **74**, 033402 (2006).